1998-10-15

Effect of salinity on density in the Leeuwin Current System

Batteen, Mary L.

Journal of Geophysical Research, Vol. 103, No. C11, pp. 24,693-24,721, October 15, 1998.
http://hdl.handle.net/10945/47164

JOURNAL OF GEOPHYSICAL RESEARCH, VOL. 103, NO. C11, PAGES 24,693–24,721, OCTOBER 15, 1998

Effect of salinity on density in the Leeuwin Current System

Mary L. Batteen and Ming-Jer Huang
Department of Oceanography, Naval Postgraduate School, Monterey, California

Abstract. Climatological temperature and salinity fields are used to calculate the salinity contribution to density and dynamic height fields in the Leeuwin Current System (LCS). While the temperature gradient is primarily linear, with warmest water to the north, the salinity fields are spatially inhomogeneous. A comparison of density fields, calculated with constant and variable salinity, shows that, off Western Australia, the density field is primarily determined by temperature. Off southwestern Australia, the density field is dependent on warm and salty (subtropical) and fresh and cold (sub-Antarctic) water masses. While the dynamic height fields, calculated with constant and variable salinity, show similar flow patterns off Western Australia, different flow patterns are found off southwestern Australia. In addition to the analysis of climatological fields, a primitive equation ocean model is used in a process-oriented study to investigate the role of salinity in the formation of currents and eddies in the LCS. Two identical ocean models, one with a climatological salinity field and the other with no horizontal salinity gradients, are run and compared with each other. Despite the model runs being initialized with similar temperature distributions, there are relatively large temperature and density differences in the southwestern Australian region due to the advection of water masses by the Leeuwin Current. On the basis of the climatological analyses and the results of the model experiments, it is concluded that, descriptively and dynamically, both temperature and salinity are essential to accurately characterize the large-scale circulation of the LCS.

1. Introduction

At a given pressure the density of seawater depends on temperature and salinity. Except for high-latitude regions and in the vicinity of sources and sinks of salt, temperature is usually considered to vary more than salinity in the upper ocean and is generally considered to be the major source of density variations [*Pickard and Emery*, 1990].

Recent dynamic height analyses by *Batteen et al.* [1995] have shown that the distribution of salinity in the California Current System (CCS) can be important in defining the large-scale circulation of the CCS. In particular, the mean variability of salinity has been shown to be responsible for a significant equatorward component along the coast of California and a strong offshore component adjacent to Baja. *Batteen et al.* [1995] concluded that, descriptively and dynamically, both temperature and salinity are essential to accurately characterize the large-scale structure of the CCS.

Besides the CCS, other eastern boundary current (EBC) regions, such as the Leeuwin Current System (LCS), could show significant changes if salinity as well as temperature effects are considered. The Leeuwin Current is an anomalous EBC that flows poleward (against the prevailing wind direction) along the Western Australian coast, down to Cape Leeuwin (See Figure 1 for geographical locations), and swings eastward extending as far east as the Great Australian Bight [e.g., *Cresswell and Golding*, 1980]. There is general agreement [e.g., *Godfrey and Ridgway*, 1985; *Smith et al.*, 1991] that the Leeuwin Current is generated by a meridional pressure gradient, which overwhelms the opposing wind stress. The source for the Leeuwin Current water is predominantly geostrophic inflow from the west due to the poleward increase of surface density [e.g., *McCreary et al.*, 1986; *Thompson*, 1987] and is augmented by a source from the North West Shelf [e.g., *Gentilli*, 1972], possibly having its origin in the Pacific Ocean [*Godfrey and Ridgway*, 1985; *Hirst and Godfrey*, 1993].

Since the Leeuwin Current is set up by geostrophic inflow from alongshore density gradients offshore, both temperature and salinity could contribute to its development. While the temperature gradient is primarily linear, with warmest water to the north, the salinity distribution is spatially inhomogeneous (Figure 2). Off Western Australia, low-salinity water is present to the north and northwest, high salinity is to the southwest, and low salinity is to the south. Depending on the time of year, these water masses could contribute to the development of the Leeuwin Current, subsurface currents, and eddies.

Here we ask the question whether salinity variability is an important consideration for defining the large-scale circulation of the LCS. To quantify the importance of salinity in the LCS, we calculate its contribution to density and to dynamic height in the LCS (section 2). After incorporating salinity into an ocean model, two identical ocean models, one with a climatological salinity field and the other with no temporal or spatial salinity gradients, are run and compared with each other (section 3). Although the results with variable salinity included show similar features to the results with uniform salinity off Western Australia, there are important quantitative differences in the Cape Leeuwin and southwestern Australian regions. The low- and high-salinity tags in the LCS are found to be particularly useful for identifying the contributions of the different water masses to the development of the Leeuwin Current and eddies.

Paper number 98JC01373.

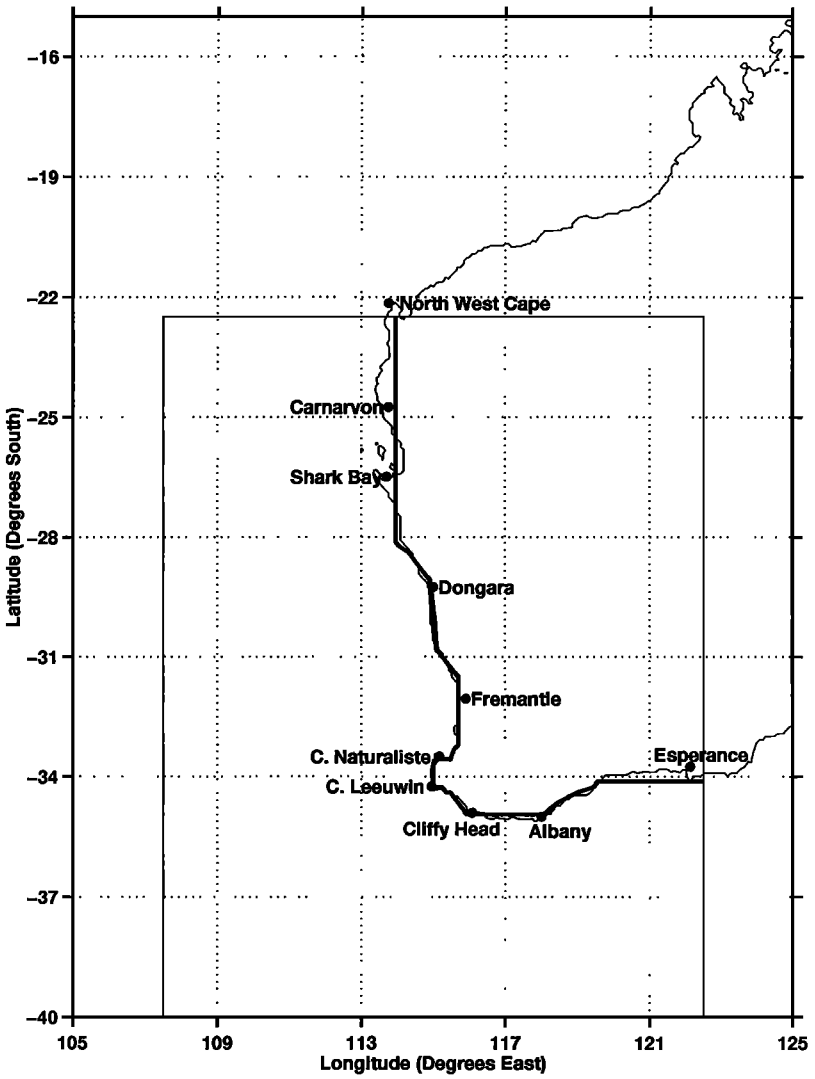

Figure 1. Domain of the model for the Leeuwin Current System (LCS) off Western Australia and southwestern Australia (inset). Domain is bounded by 22.5°S to 40°S, 107.5°E to 122.5°E. The irregular coastline (solid line) used in the model is also shown, along with geographic locations.

2. Analysis of Hydrographic and Dynamic Height Fields

2.1. Analysis of Annual Hydrographic and Dynamic Height Fields

Two major water masses occur for all or part of the year off Western Australia (Figure 2): a warm (tropical) low-salinity water mass from the North West Shelf [e.g., *Weaver and Middleton*, 1989], possibly having its origins in the Pacific Ocean [*Godfrey and Ridgway*, 1985; *Hirst and Godfrey*, 1993], and a cooler (subtropical), higher-saline water mass offshore that is influenced by the presence of a large, semipermanent trough extending in a northeastward direction [*Andrews*, 1977].

The seas just south of Cape Leeuwin and eastward to the entrance (near Esperance in Figure 2) to the Great Australian Bight are influenced by several water types: (1) subtropical water from west of Western Australia in summer [*Andrews*, 1977], (2) tropical water from north of Western Australia in autumn and winter [*Rochford*, 1969; *Cresswell and Golding*, 1980], and (3) local sub-Antarctic water characterized by its coldness and low salinity [*Rochford*, 1986].

To explore the water masses of this area, the climatological data sets of *Levitus et al.* [1994] and *Levitus and Boyer* [1994] were employed. The data are gridded with 1° horizontal resolution at standard depth levels. These data sets, which include annual and monthly mean temperature and salinity fields, were used to compute annual and seasonal density and dynamic height fields.

Before presenting the annual and monthly climatological temperature, salinity, density, and dynamic height fields, we describe how the calculations for density and dynamic height were obtained. Following *Batteen et al.* [1995], the density is computed using the following approximate equation of state for seawater:

$$\rho = \rho_0[1 - \alpha(T - T_0) + \beta(S - S_0)],$$

where α and β are the expansion and contraction coefficients for temperature T and salinity S, respectively; ρ is density; S_0 is the reference salinity; and T_0 is the reference temperature. This equation can estimate the effect of salinity for a given region if typical values of α, β, T_0, and S_0 are used. For the

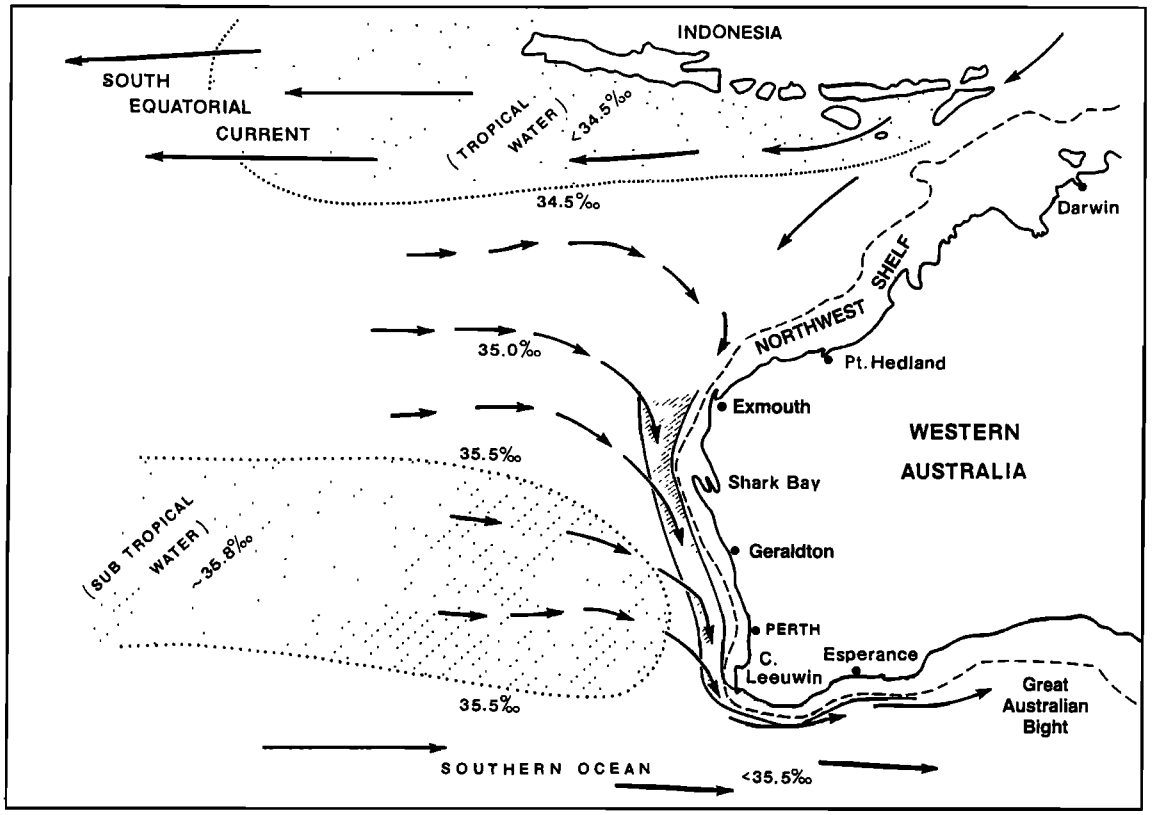

Figure 2. Schematic chart of the mean large-scale circulation in the eastern Indian Ocean. The tropical (salinity <34.5) and subtropical (>35.8) water masses are dotted. The edge of the continental shelf (200 m isobath) is dashed. The Leeuwin Current is the southward flow of warm low-salinity water down the Western Australian coast [from *Pearce and Cresswell*, 1985].

LCS region, α is chosen to be 2.5×10^{-4} $(°K)^{-1}$, β is 7.5×10^{-4}, T_0 is 278.2°K, and S_0 is 35.5 practical salinity units (psu).

To assess the effect of salinity on density in the LCS, we calculate density in the above equation for variable and uniform salinity. Calculating density for variable salinity means that the density in the above equation is computed at a given level with climatological values of both T and S. Calculating density for uniform salinity means that the density in the above equation computes only climatological values of T at a given level and has S replaced by S_0, so that it reduces to

$$\rho = \rho_0[1 - \alpha(T - T_0)].$$

To assess the effect of salinity gradients on the large-scale ocean circulation of the LCS, dynamic height fields are calculated with and without the inclusion of salinity variations. Note that since these calculations use 1° horizontal resolution; they are too coarse to adequately resolve the Leeuwin Current which is $O(100)$ km wide. (In section 3 the Leeuwin Current is adequately resolved in a modeling study that uses 11 by 14 km horizontal resolution.) Such calculations, however, can be successfully used to infer the general directions for geostrophic flow, which subsequently set up the currents in the LCS. The dynamic height anomaly $\Delta\Phi$ is calculated by integrating the specific volume anomaly δ over depth and comparing it with $\Delta\Phi_{35.5TP}$ (where the subscripts 35.5, T, and P stand for salinity 35.5 psu, temperature, and pressure, respectively), calculated by integrating δ_T. Comparisons between horizontal gradients of $\Delta\Phi$ and $\Delta\Phi_{35.5TP}$ are used to provide insight concerning the importance of salinity variations to the flow field. The reference level used in this study is 1000 m depth.

The climatological annual mean temperature fields are shown at 10, 100, 200, and 400 m depth in Figure 3a. At all depths shown, the temperature distribution is primarily zonal, with the isotherms running roughly east-west. Maximum temperatures are in the north and decrease to the south. The temperature differences from north to south are ~11°C, 9°C, 7°C, and 2°C at 10, 100, 200, and 400 m depth, respectively.

The climatological annual mean salinity fields are shown at 10, 100, and 400 m depth in Figure 3b. The common features of the 10 and 100 m depth plots can be clearly seen: low-salinity (tropical) water to the north and northwest, high-salinity (subtropical) water to the southwest, and low-salinity (sub-Antarctic) water to the south. The maximum salinity for 10 m depth is centered at ~32°S, while the maximum salinity for 100 m depth is centered at ~28°S. The salinity gradient weakens from 10 to 100 m depth. The 35.5 salinity contour extends all along southwestern Australia at 10 m depth, but only as far east as Albany at 100 m depth. At 200 m depth the salinity pattern is similar to the zonal temperature pattern, with maximum salinity in the north and minimum salinity in the south. At this depth the 35.5 salinity contour extends only as far south as Fremantle (~32°S). At 400 m depth the salinity difference is only 0.4 psu from north to south.

The annual density fields calculated with uniform (variable) salinity at 10, 100, 200, and 400 m depth are shown in Figure 3c (Figure 3d). Note that, in general, the range of density at each

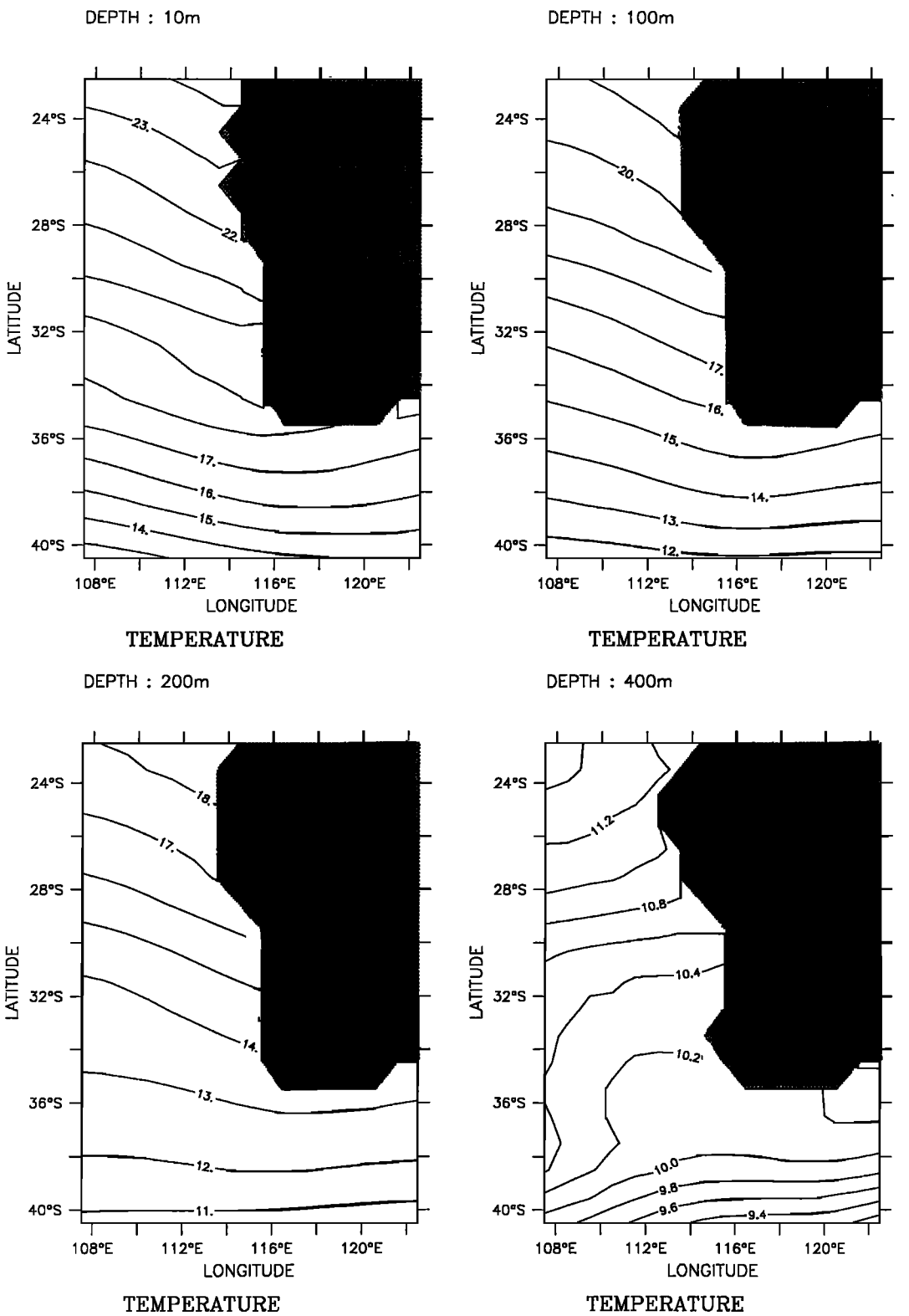

Figure 3a. Annual temperature fields at 10, 100, 200, and 400 m depth. For 10, 100, and 200 m depth, the contour interval is 1°C, and for 400 m depth, it is 0.2°C.

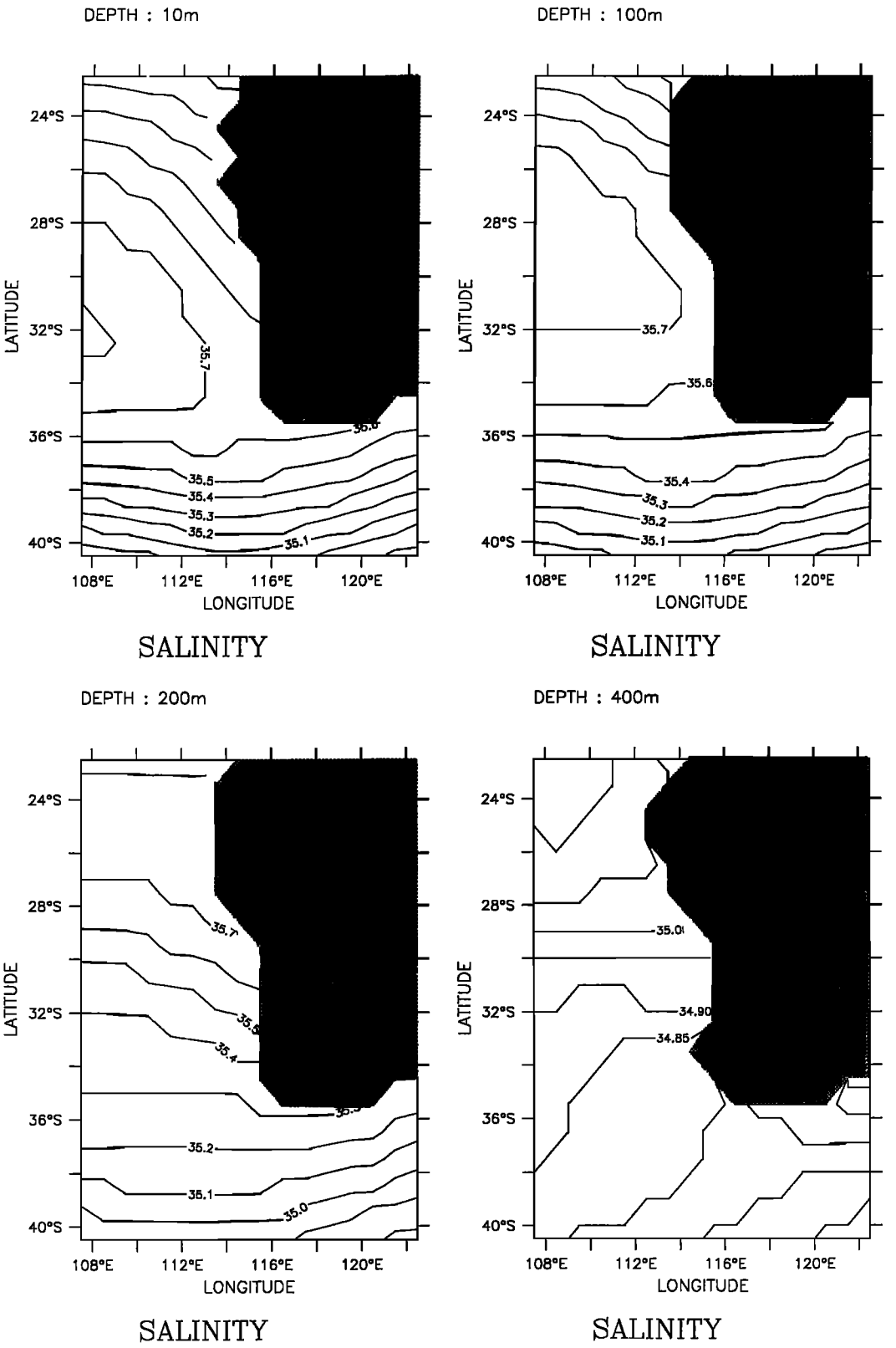

Figure 3b. Annual salinity fields at 10, 100, 200, and 400 m depth. For 10, 100, and 200 m depth, the contour interval is 0.1 psu, and for 400 m depth, it is 0.05 psu.

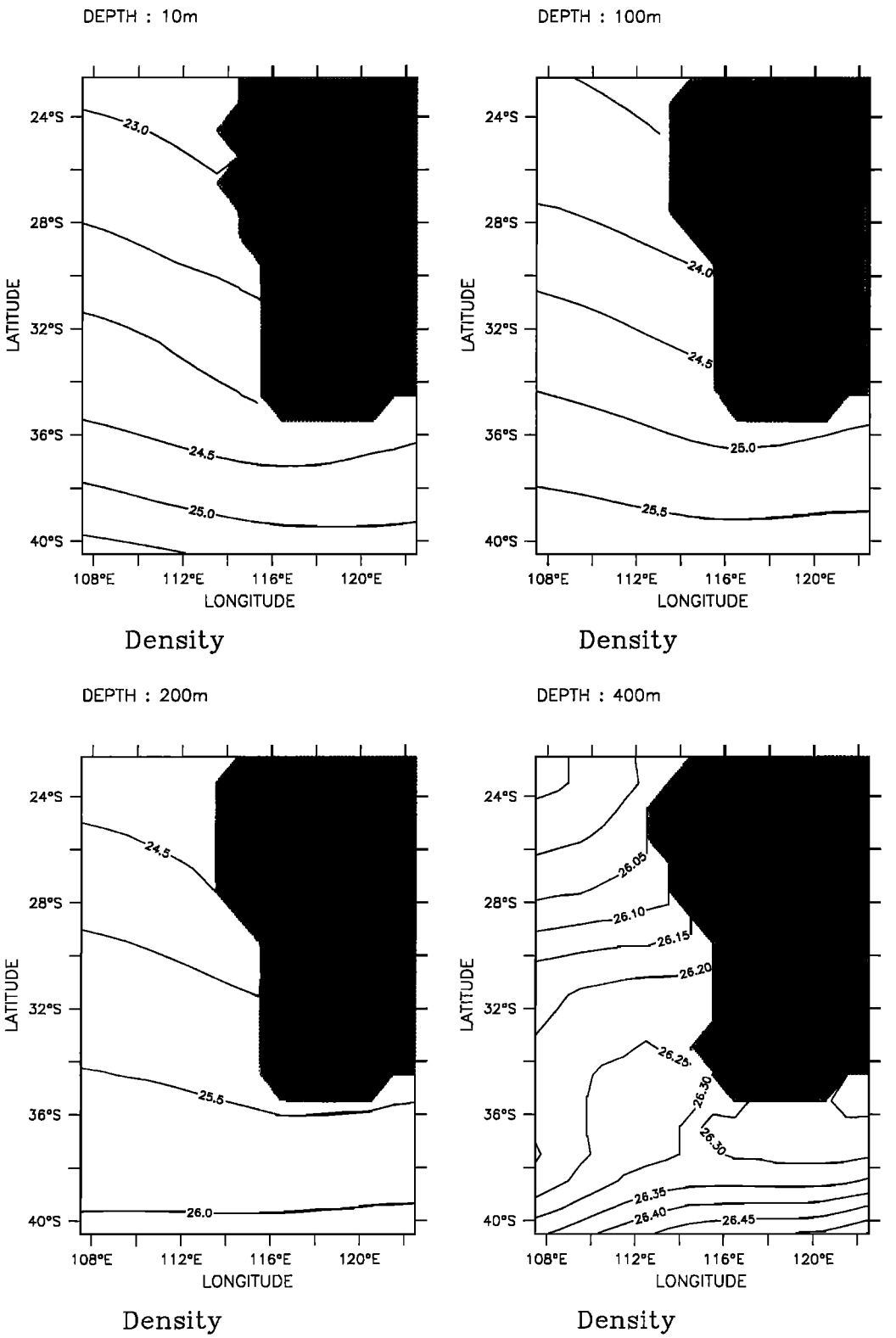

Figure 3c. Annual density field $\sigma_{\pm}$ with uniform salinity at 10, 100, 200, and 400 m depth. For 10, 100, and 200 m depth, the contour interval is 0.5 psu, and for 400 m depth, it is 0.05 psu.

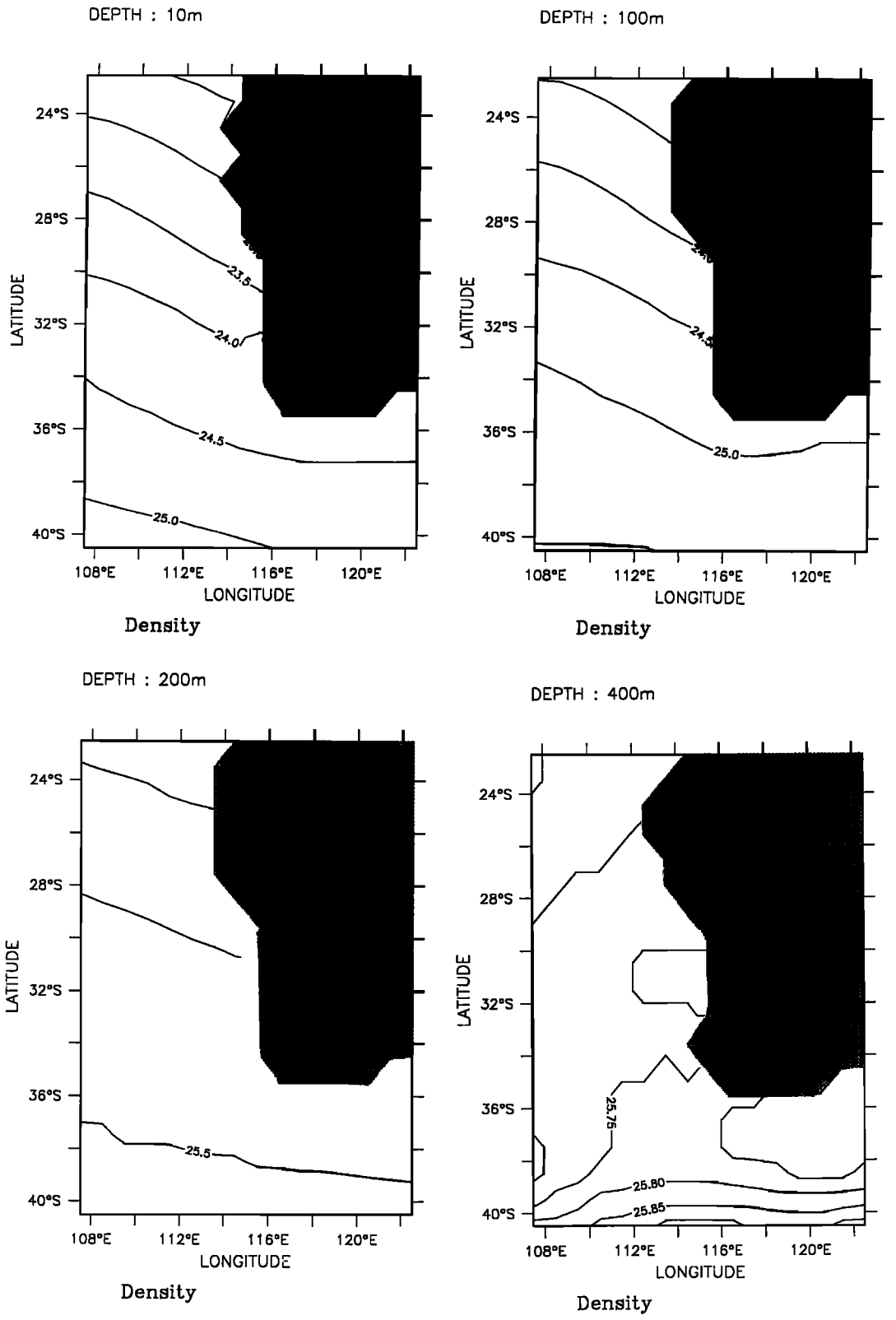

Figure 3d. Same as Figure 3c, but for variable salinity.

level is greater for the case in which uniform salinity is used. A comparison of the upper levels (i.e., 10 and 100 m depth) in Figures 3c and 3d shows the following. Although, off Western Australia, the density is primarily determined by the temperature field, the density fields in Figure 3d are generally less dense than those in Figure 3c owing to the presence of the low-salinity (tropical) water mass. South of ~34°S, the effect of salinity on density becomes significant. In particular, off southwestern Australia, the density is influenced by both the warm and salty (subtropical) water mass and the fresh and cold (sub-Antarctic) water mass. At 200 m depth the density in Figure 3d is generally greater than that in Figure 3c owing to the presence of high salinity throughout the region. At 400 m depth the density field in Figure 3c and 3d is relatively uniform throughout the region.

Figures 4a and 4b show the annual dynamic height patterns at 10, 100, 200, and 400 m depth for uniform salinity, i.e., $\Delta\Phi_{35\ 5TP}$, and for variable salinity, i.e., $\Delta\Phi$, respectively. In both figures the upper level dynamic height contours tend to be perpendicular to the west coast of Australia, which is consistent with onshore geostrophic flow toward Western Australia. Between 34°S and 36°S, while the upper level dynamic height fields in Figure 4a tend to be zonally distributed, those in Figure 4b tend to vary in both the meridional and zonal directions owing to the influence of the salty (subtropical) water mass offshore. The lower level dynamic height patterns in Figures 4a and 4b show equatorward flow off Western Australia, which is consistent with the depths at which the equatorward undercurrent has been observed [e.g., *Thompson*, 1984].

2.2. Analysis of Seasonal Hydrographic and Dynamic Height Fields

Since the LCS has a strong seasonal (e.g., the Leeuwin Current is strongest from March to August) as well as annual signal, the monthly mean temperature and salinity climatological fields are examined to evaluate the effects of the seasonal evolution of salinity on the density and dynamic height fields. The annual mean temperature and salinity fields showed that the water mass characteristics of the LCS are very similar at 10 and 100 m depth. Since the seasonal cycle has essentially the same vertical pattern in the upper layers, we present only the 10 m depth seasonal fields here.

The same three water masses described earlier are discussed here to help identify how salinity seasonally influences the density and dynamic height fields. These water masses are the warm and fresh tropical water mass off northwestern Australia, the warm and salty subtropical water mass off southwestern Australia, and the cold and fresh water mass off southwestern Australia.

Figure 5a shows the monthly mean temperature fields in February, May, August, and November. As the November and February plots show, the temperature gradient off Western Australia during the austral spring and summer has a 45° slope from northeast to southwest, which provides the source for an onshore geostrophic current (i.e., the Leeuwin Current). As the May and August plots show, the slope becomes even steeper during the austral fall and winter, which is consistent with the Leeuwin Current being strongest during this period. Off southwestern Australia, except for the advection of the Leeuwin Current in the vicinity of Cape Leeuwin during the austral fall and winter, the temperature pattern follows a typical seasonal cycle of warmest (coldest) temperature off the coast in summer (winter).

Figure 5b shows the monthly mean salinity fields in February, May, August, and November. In February the salinity field shows a zonal distribution of fresh water in the north, which becomes saltier poleward to ~32°S. There is an offshore region of maximum salinity of ~35.8 from ~28°S to 35°S, centered at ~32°S. South of ~35°S, fresher water is found. In May the salinity gradient has a 45° slope off Western Australia. The maximum salinity has shifted southward to ~34°S. In August the fresh water off northwestern Australia has moved farther southward, while the maximum salinity has moved farther offshore. In November, off northwestern Australia, the fresh water has been replaced by more saline water. The maximum salinity has retreated equatorward to ~31°S.

The density fields shown in Figures 6a and 6b were calculated with uniform and variable salinity, respectively. In general, throughout the year, the density fields off Western Australia in Figure 6b are less dense than those in Figure 6a owing to the presence of low-salinity (tropical and sub-Antarctic) water masses. In the southwestern Australia region the density fields in Figure 6b are more dense than those in Figure 6a because of the presence of the salty (subtropical) water mass. Note that south of 36°S, the density gradient is enhanced in the case with uniform salinity (Figure 6a).

Figures 7a and 7b show the seasonal dynamic height patterns for uniform and variable salinity, respectively. In both figures, throughout the year, off Western Australia, the dynamic height flow pattern is consistent with onshore geostrophic flow toward Western Australia. In contrast, south of 36°S, while the dynamic height fields in Figure 7a tend to be zonally distributed throughout the year, those in Figure 7b tend to vary in both the meridional and zonal directions owing to the influence of the salty (subtropical) water mass offshore. Note that south of 36°S, there is an enhanced dynamic height in the case with uniform salinity (Figure 7a).

To quantify the seasonal effect of salinity on the dynamic height field, the dynamic height fields at several offshore and nearshore locations were calculated. Figure 8 shows the meridionally averaged dynamic height field at 108.5°E from regions (1) 22°S to 29°S, (2) 30°S to 35°S, and (3) 36°S to 40°S. In region 1 the dynamic height with variable salinity (solid line) is similar to that with uniform salinity (dashed line). In the other two regions the dynamic height fields are dependent on both temperature and salinity from approximately May to August in region 2 and for most of the year in region 3. In region 2 the seasonal dependence on both temperature and salinity coincides with the time frame that the Leeuwin Current is strongest. In region 3 the seasonal salinity effect is consistent with the time that the subtropical salty water moves poleward to ~40°S.

The dynamic height fields calculated at several nearshore locations are shown in Figure 9. In nearshore regions 1 and 2, which correspond to coastal locations off Western Australia, because the salinity gradient is not as strong as in the offshore regions, the salinity effect is not very significant. In contrast, in nearshore region 3, which corresponds to a coastal location off southwestern Australia, the dynamic height is dependent on both temperature and salinity throughout most of the year, indicating that in this region, salinity plays a very important role.

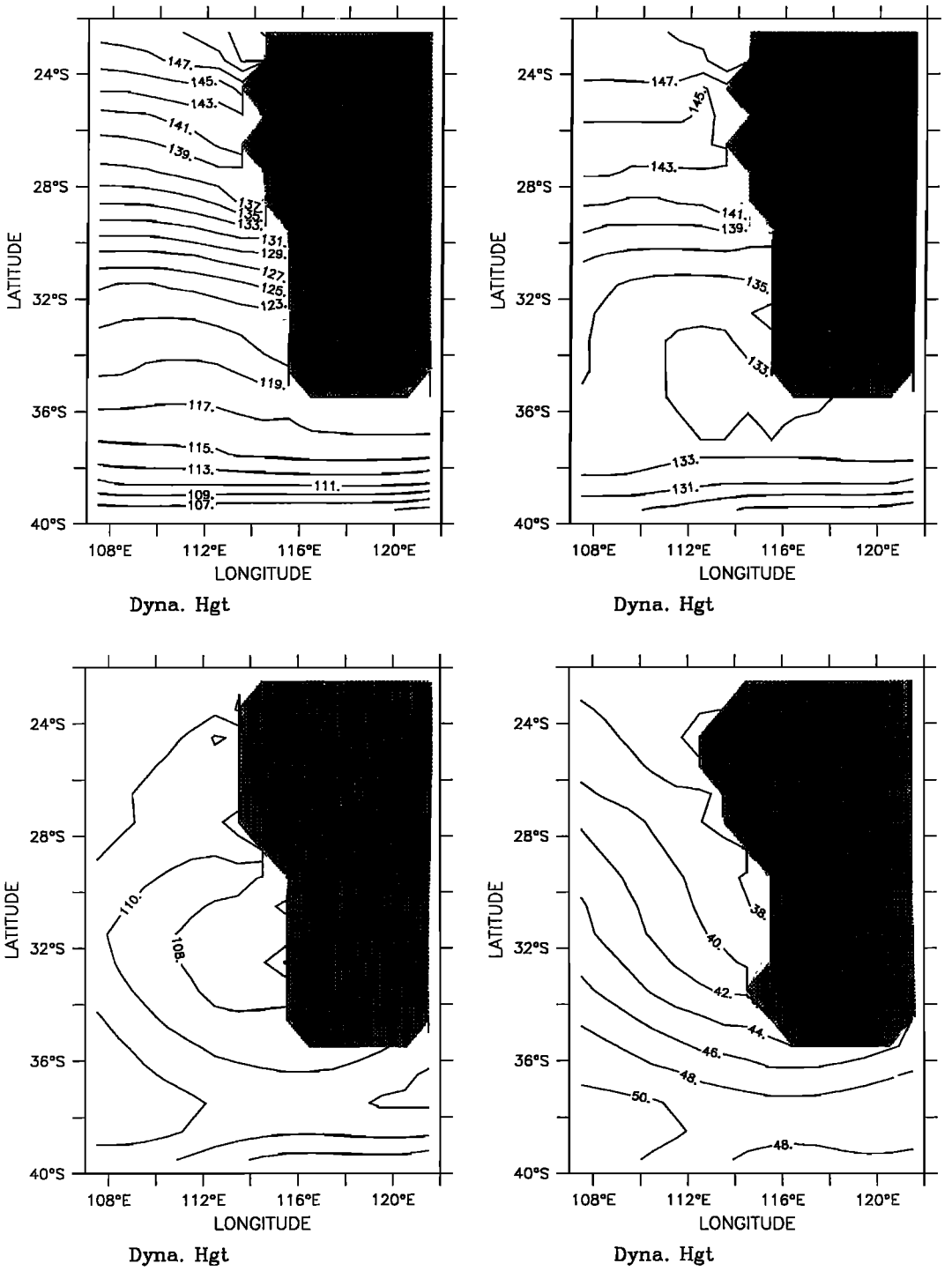

Figure 4a. Annual dynamic height field with uniform salinity at 10, 100, 200, and 400 m depth. The contour interval is 2 dynamic centimeters (dyn. cm.).

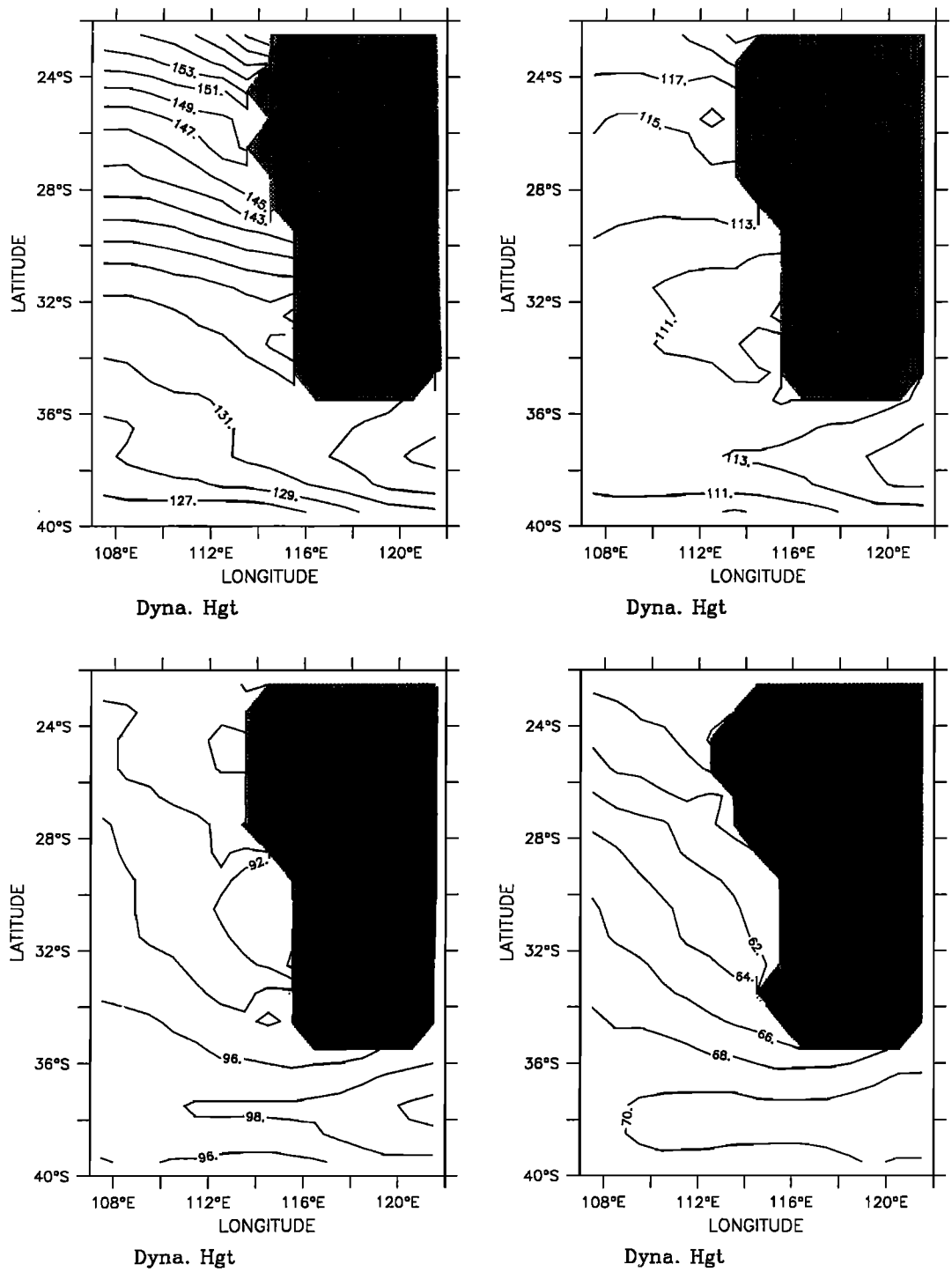

Figure 4b. Same as Figure 4a, but for variable salinity.

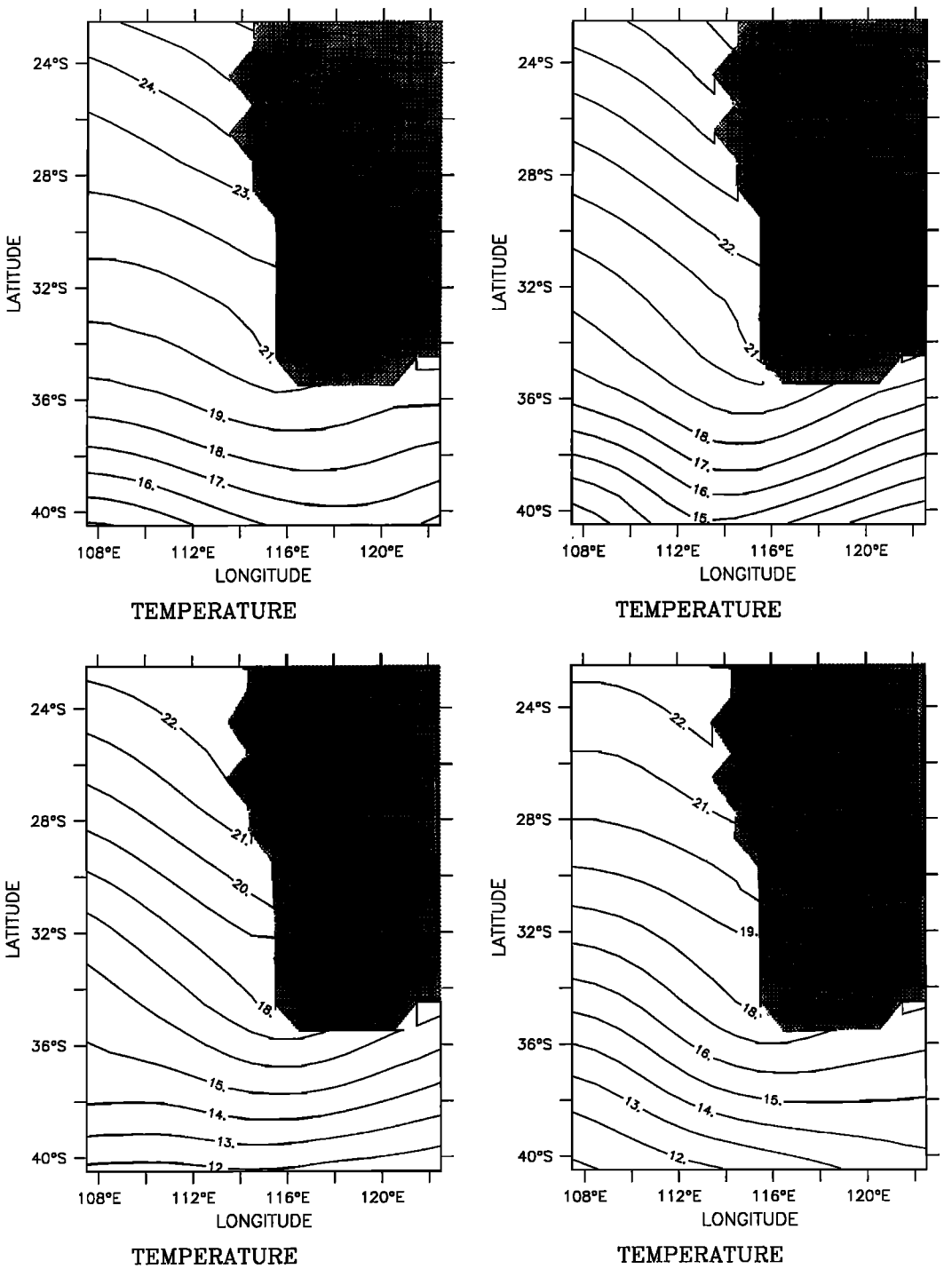

Figure 5a. Climatological seasonal temperature fields at 10 m depth in (top left) February, (top right) May, (bottom left) August, and (bottom right) November. The contour interval is 1°C.

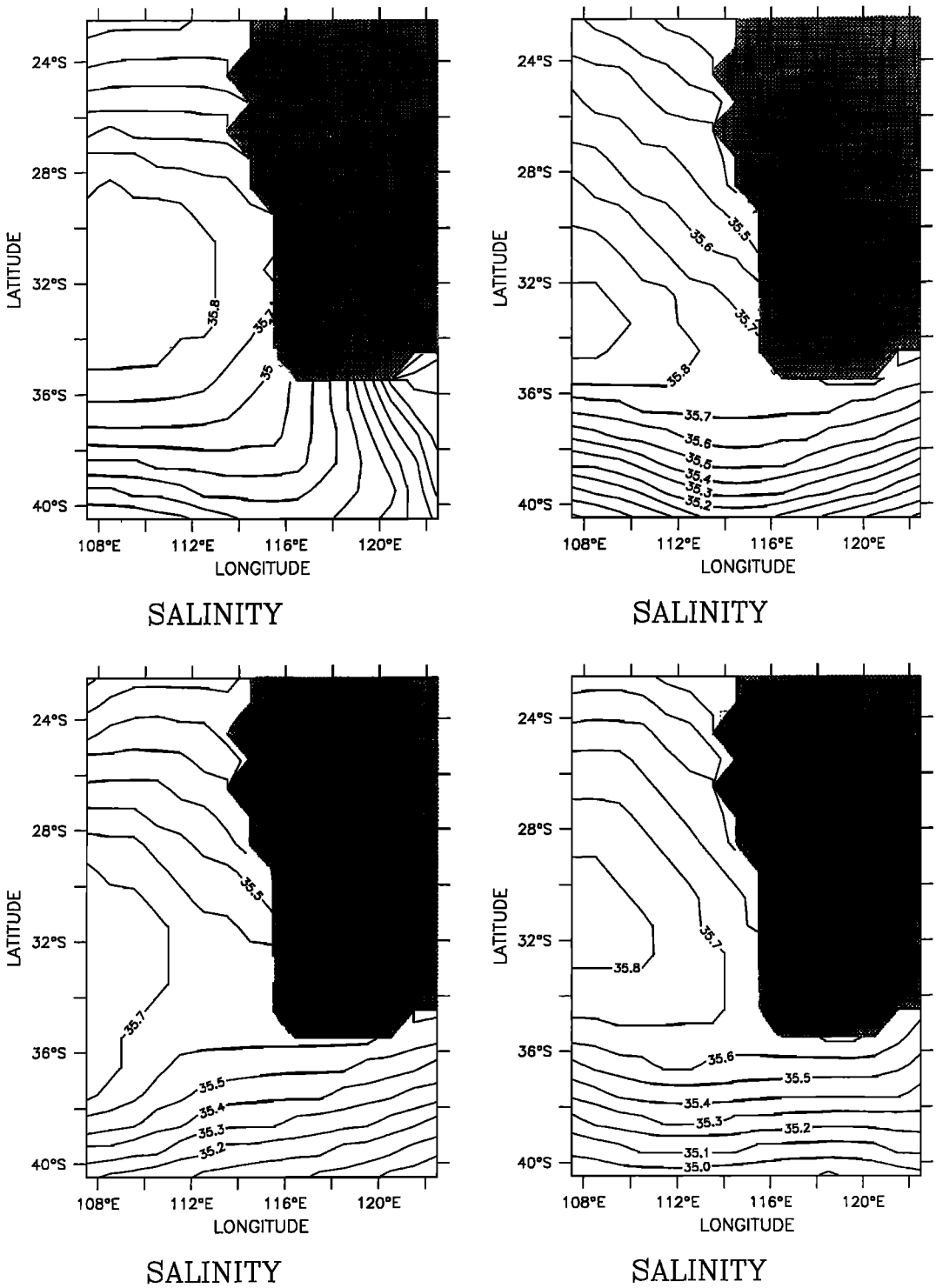

Figure 5b. Same as Figure 5a, but for salinity.

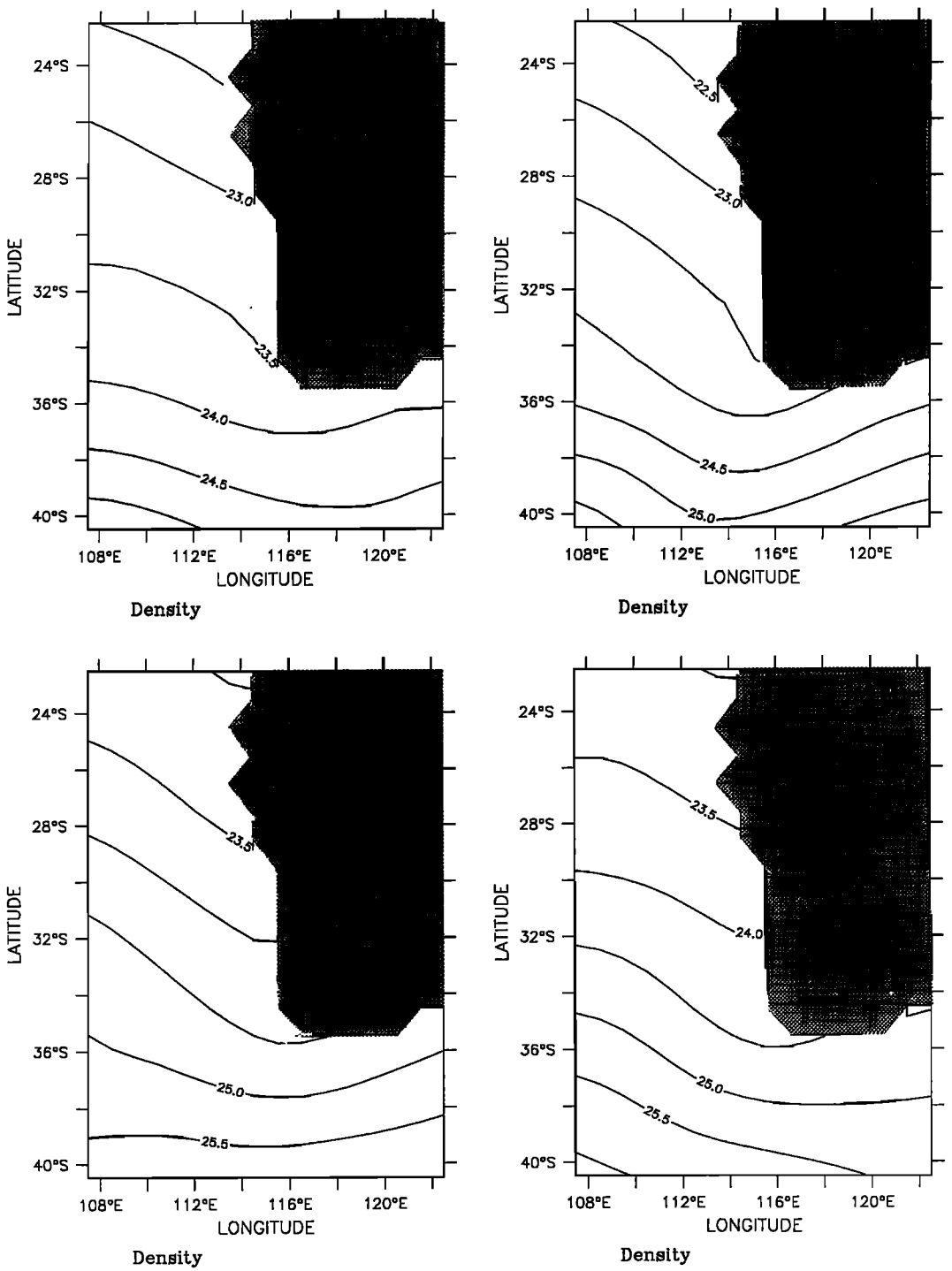

Figure 6a. Seasonal density σ_t fields with uniform salinity at 10 m depth in (top left) February, (top right) May, (bottom left) August, and (bottom right) November. The contour interval is 0.5.

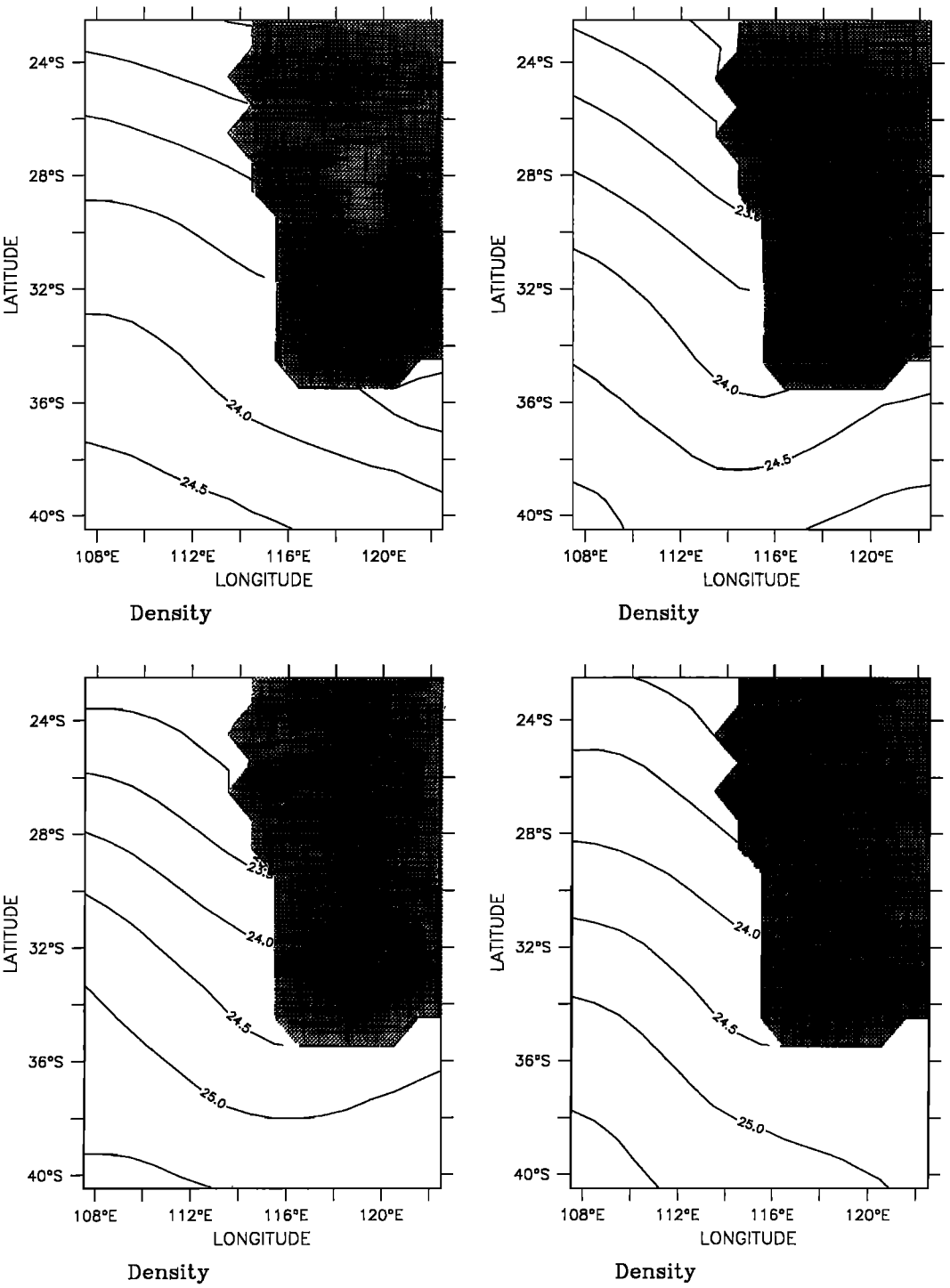

Figure 6b. Same as Figure 6a, but for variable salinity.

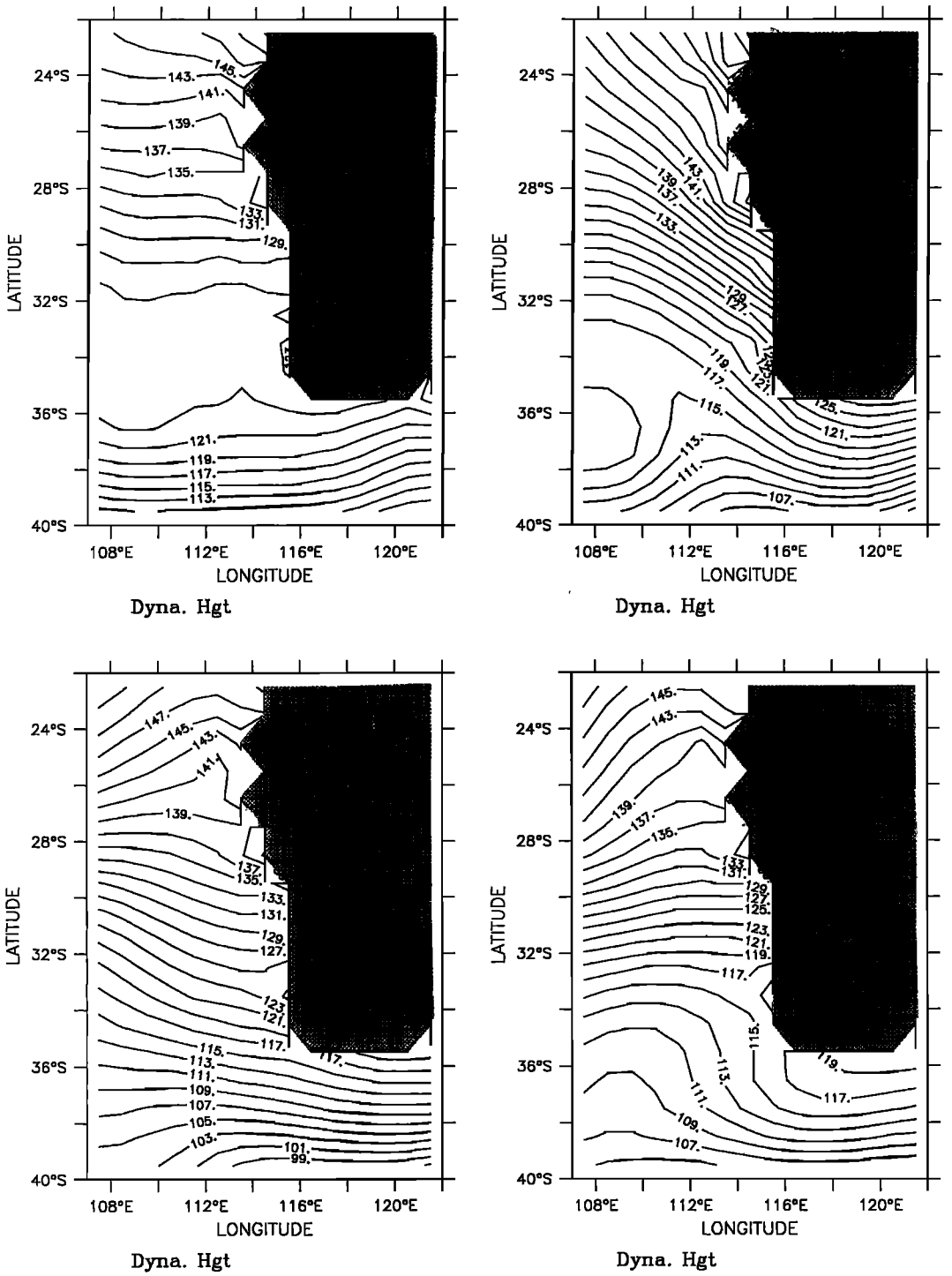

Figure 7a. Seasonal dynamic height fields with uniform salinity at 10 m depth in (top left) February, (top right) May, (bottom left) August, and (bottom right) November. The contour interval is 2 dyn. cm.

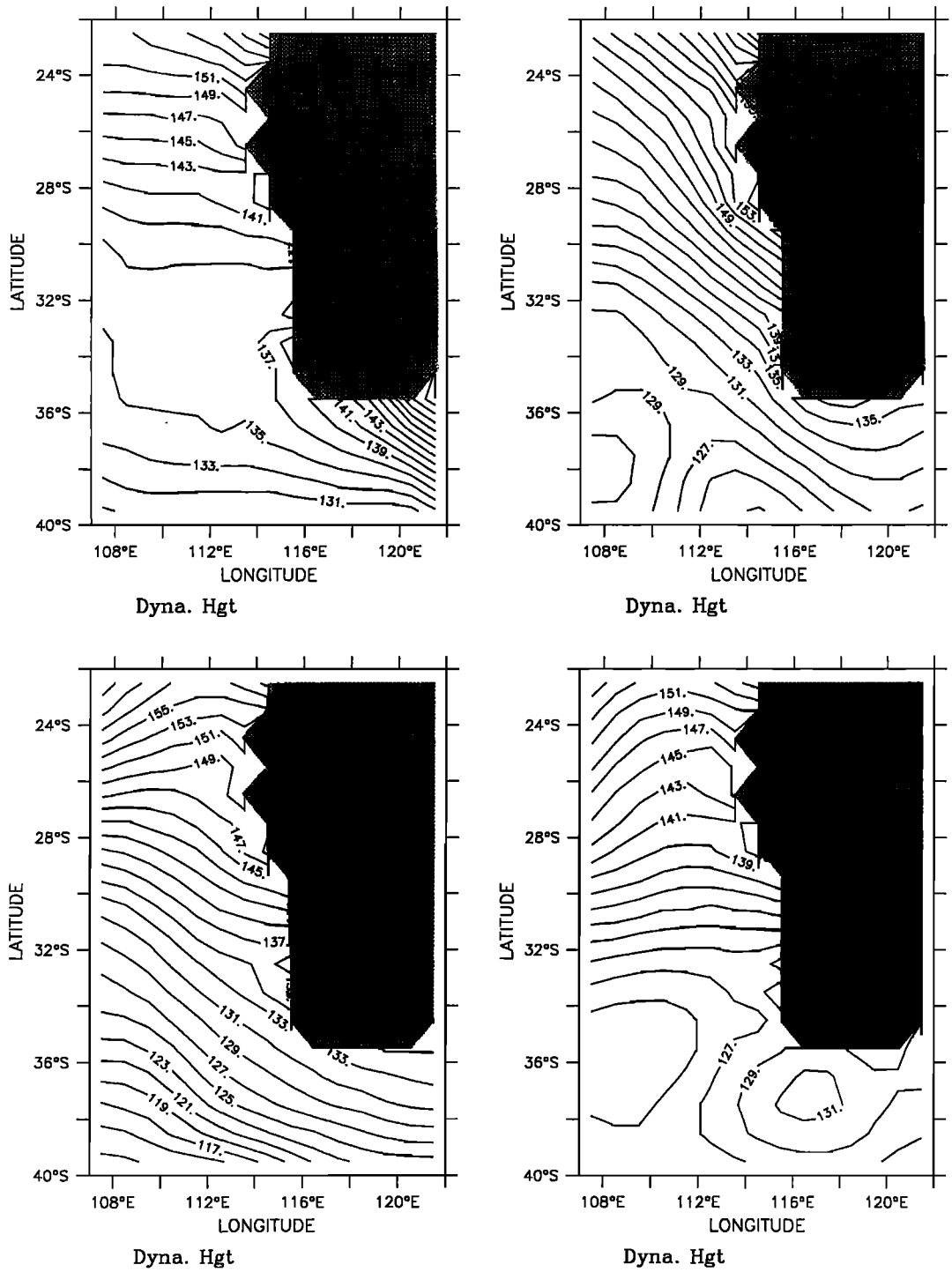

Figure 7b. Same as Figure 7a, but for variable salinity.

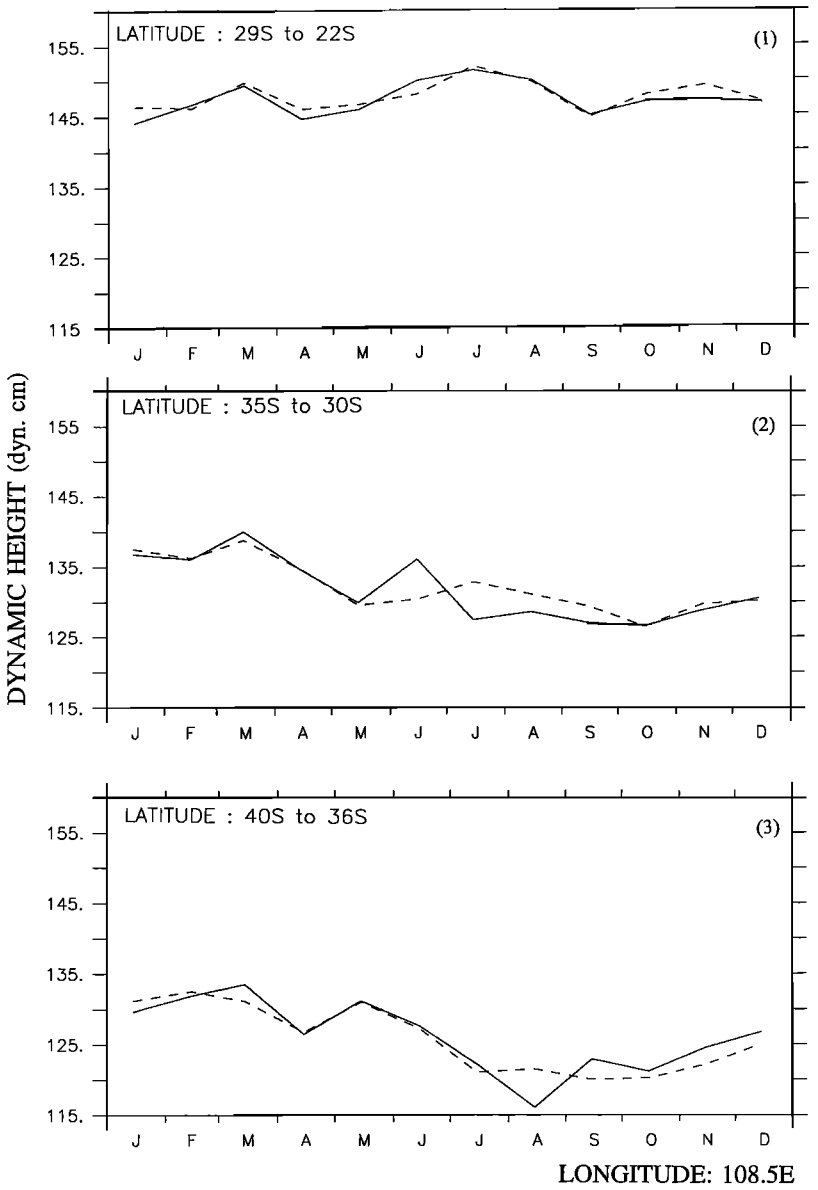

Figure 8. Seasonal dynamic height fields meridionally averaged at 108.5°E from (top) region 1, 22°S to 29°S; (middle) region 2, 30°S to 35°S; and (bottom) region 3, 36°S to 40°S. The dashed (solid) line refers to dynamic height calculated with uniform (variable) salinity.

3. Effect of Salinity on an Ocean Model of the LCS

3.1. Model

3.1.1. Model description. The numerical model in this study was originally used for a coarse resolution, closed basin by *Haney* [1974] and later adapted for eddy-resolving, limited EBC regions with open borders on the northern, western, and eastern boundaries by *Batteen et al.* [1989] and *Batteen* [1997] and also for southern boundaries by *Batteen and Butler* [1998]. The limited area EBC model is multilevel, uses nonadiabatic primitive equations on a beta plane, and has both baroclinic and barotropic velocity components. The model is based on the hydrostatic, Boussinesq, and rigid lid approximations. The governing equations are as follows:

$$\frac{du}{dt} = \frac{-1}{\rho_0}\frac{\partial \rho}{\partial x} + fv - A_M\nabla^4 u + K_M\frac{\partial^2 u}{\partial z^2} \quad (1)$$

$$\frac{dv}{dt} = \frac{-1}{\rho_0}\frac{\partial \rho}{\partial y} - fu - A_M\nabla^4 v + K_M\frac{\partial^2 v}{\partial z^2} \quad (2)$$

$$\frac{\partial u}{\partial x} + \frac{\partial v}{\partial y} + \frac{\partial w}{\partial z} = 0 \quad (3)$$

$$\frac{\partial p}{\partial z} = -\rho g \quad (4)$$

$$\rho = \rho_0[1 - \alpha(T - T_0) + \beta(S - S_0)] \quad (5)$$

$$\frac{dT}{dt} = -A_H\nabla^4 T + K_H\frac{\partial^2 T}{\partial z^2} \quad (6)$$

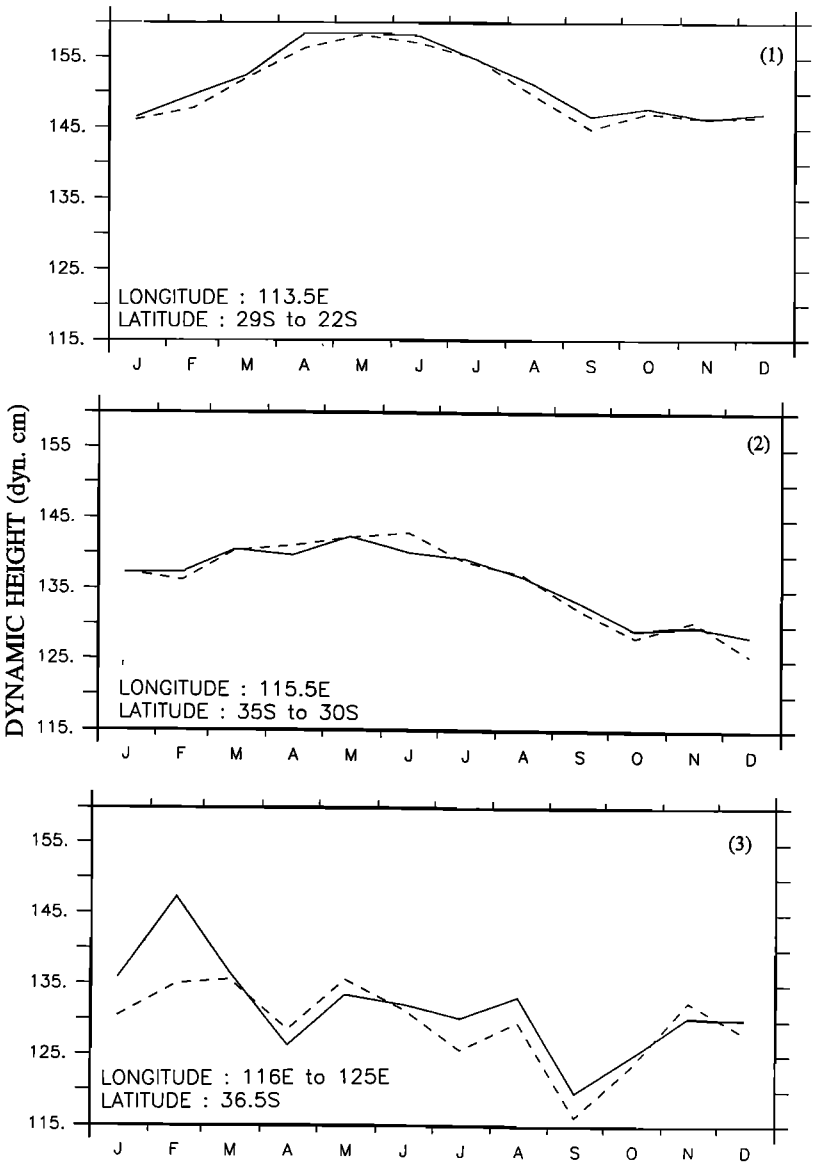

Figure 9. Seasonal dynamic height fields in the nearshore region at (top) 113.5°E, which is latitudinally averaged from 22°S to 29°S; (middle) 115.5°E, which is latitudinally averaged from 30°S to 35°S; and (bottom) 36.5°S, which is longitudinally averaged from 116°E to 125°E. The dashed (solid) line refers to dynamic height calculated with uniform (variable) salinity.

$$\frac{dS}{dt} = -A_H \nabla^4 S + K_H \frac{\partial^2 S}{\partial z^2}. \tag{7}$$

In the (1)–(7), t is time; (x, y, z) is a right-handed Cartesian coordinate system with x pointing toward shore, y pointing alongshore, and z pointing upward. The corresponding velocity components are (u, v, w), T is temperature, S is salinity, ρ is density, and p is pressure.

For finite differencing, a space-staggered B scheme [*Arakawa and Lamb*, 1977] is used in the horizontal. *Batteen and Han* [1981] have shown that this scheme is appropriate when the grid spacing is approximately on the same order as or less than the Rossby radius of deformation, which meets the criteria of this study. The horizontal grid spacing is 14 km in the north-south direction and 11 km in the east-west direction, while the internal Rossby radius of deformation is ~30 km. In the vertical the 10 layers are separated by constant z levels of 13, 46, 98, 182, 316, 529, 870, 1416, 2283, and 3656 m. This spacing scheme concentrates more on the upper, dynamically active part of the ocean, above the thermocline.

The model domain (Figure 1) is a rectangular region encompassing the west and south coasts of Australia, from ~22.5°S to 40°S (1792 km alongshore) and from ~107.5°E to 122.5°E (1408 km cross shore). The coastal boundaries of the model domain are closed and have both the tangential and normal components of velocity set to zero. Bottom topography has been omitted to focus on the roles played by alongshore temperature and salinity gradients. The constant depth used in the model is 4500 m. A modified version of the radiation boundary conditions of *Camerlengo and O'Brien* [1980] is used for the open ocean domain boundaries to the north, south, east, and west. Some spatial smoothing is applied in the vicinity of the open boundaries.

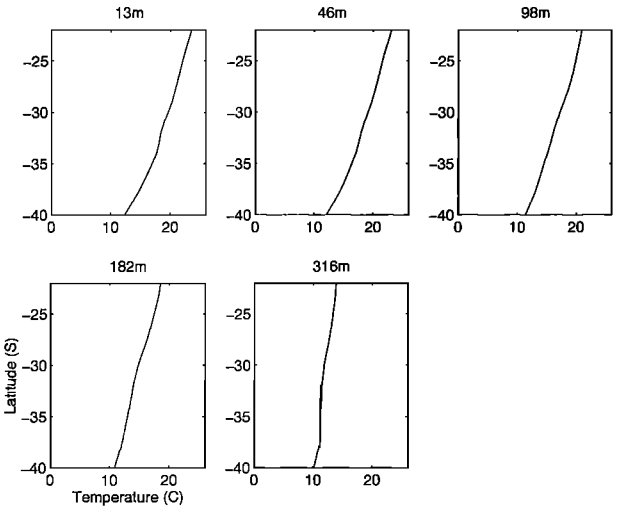

Figure 10a. Annual alongshore temperature fields for the upper five model levels. Since the lower five levels do not have much latitudinal variation, they are assumed to be horizontally uniform for each level.

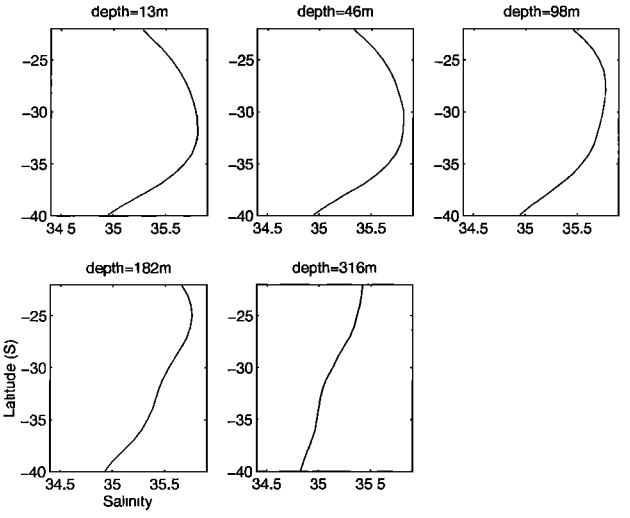

Figure 10b. Same as Figure 10a, but for salinity.

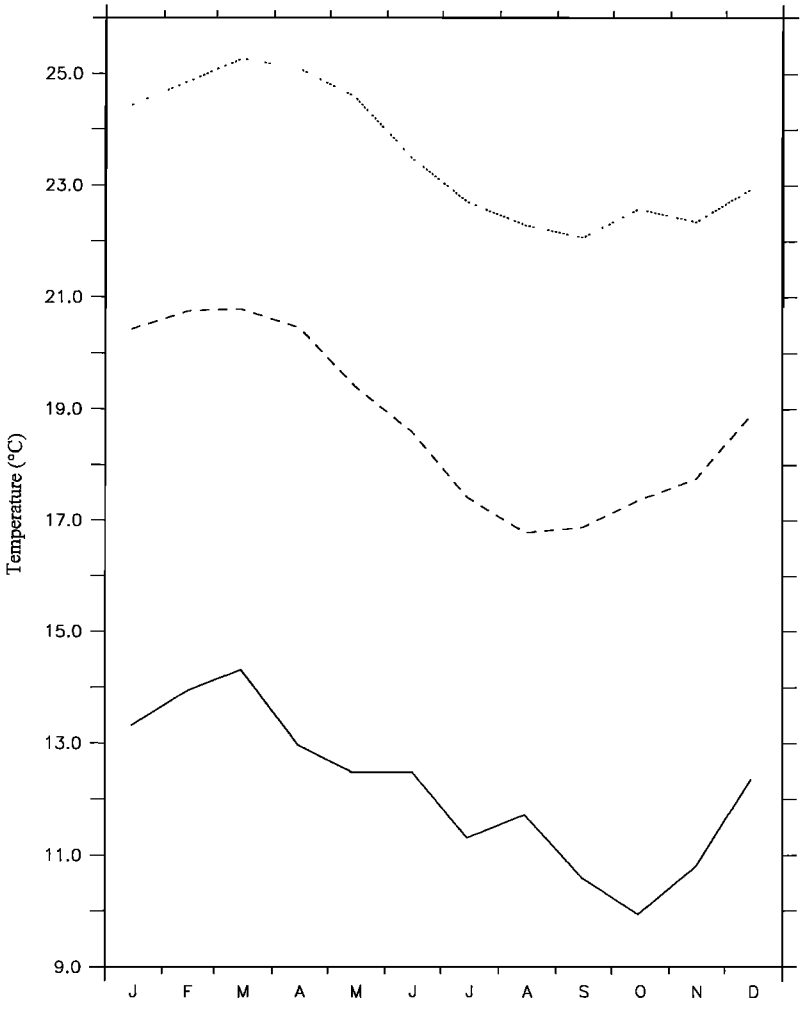

Figure 11a. Time series at 10 m depth of monthly temperature fields used as seasonal forcing in experiments 3 and 4. Solid lines are for 40°S, dashed lines are for 31.5°S, and dotted lines are for 22.5°S.

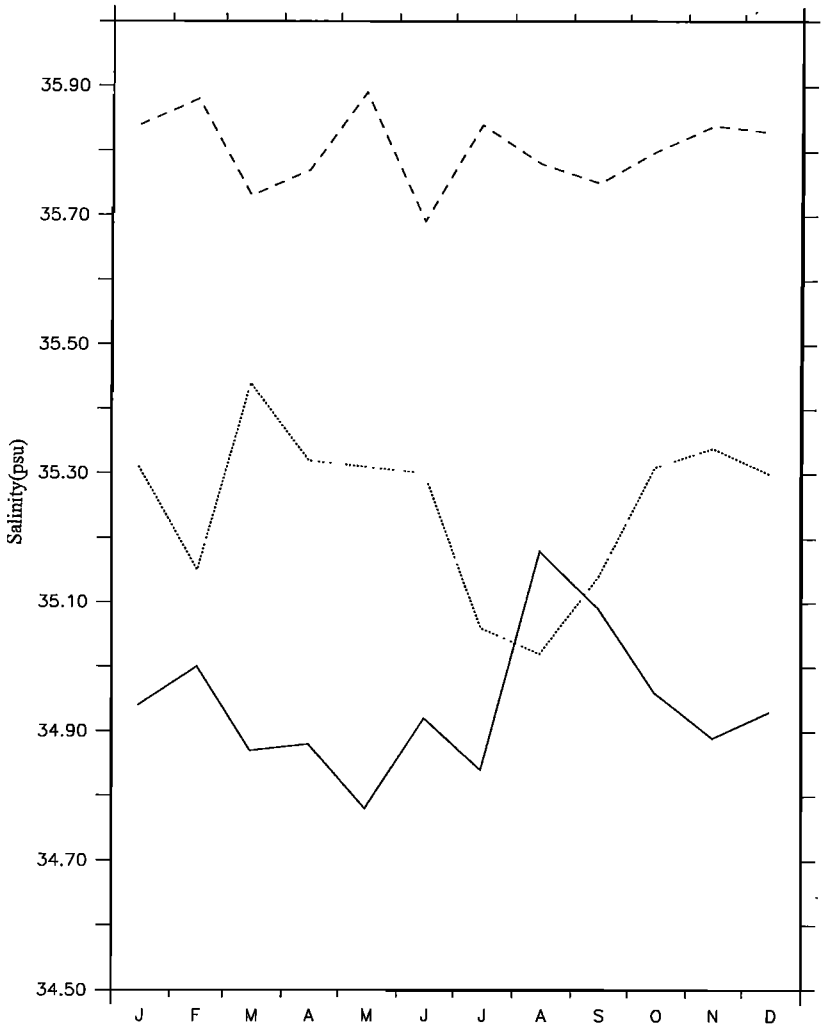

Figure 11b. Same as Figure 11a, but for salinity.

The model uses biharmonic lateral heat and momentum diffusion with the same choice of coefficients (i.e., 2.0×10^{17} $cm^4\ s^{-1}$) as used by *Batteen et al.* [1989]. *Holland* [1978] showed that the highly scale-selective biharmonic diffusion acts predominantly on submesoscales, while *Holland and Batteen* [1986] found that baroclinic mesoscale processes can be damped by Laplacian lateral heat diffusion. As a result, the use of biharmonic lateral diffusion should allow mesoscale eddy generation via barotropic (horizontal shear) and/or baroclinic (vertical shear) instability mechanisms. As in the work by *Batteen et al.* [1989], weak (0.5 $cm^2\ s^{-1}$) vertical eddy viscosities and conductivities are used. Bottom stress is parameterized by a simplified quadratic drag law [*Weatherly*, 1972], as in the study by *Batteen et al.* [1989].

The method of solution is straightforward with the rigid lid and flat bottom assumptions because the vertically integrated horizontal velocity is subsequently nondivergent. The vertical mean flow can be described by a stream function that can be predicted from the vorticity equation, while the vertical shear currents can be predicted after the vertical mean flow is subtracted from the original equations. The other variables, i.e., temperature, density, vertical velocity, and pressure, can be explicitly obtained from the thermodynamic energy equation, equation of state, continuity equation, and hydrostatic equation, respectively (for more complete details on the method of solution, see *Batteen* [1997]).

3.1.2. Forcing conditions and experimental design. Previous experiments by *Batteen and Rutherford* [1990] investigated the role of alongshore temperature gradients in generating the Leeuwin Current and eddies off Western Australia with a model domain that was a closed eastern boundary with open borders to the north, south, and west. The model was initialized with climatological temperature fields from *Levitus* [1982], and the ocean was then allowed to geostrophically adjust in the absence of winds (roughly analogous to the true

Table 1. The Design of the Experiments

Experiment	Description
	Response To Mean Forcing
1	variable alongshore temperature gradients with horizontally uniform salinity gradients
2	variable alongshore temperature and salinity gradients
	Response To Seasonal Forcing
3	variable alongshore temperature gradients with horizontally uniform salinity gradients
4	variable alongshore temperature and salinity gradients

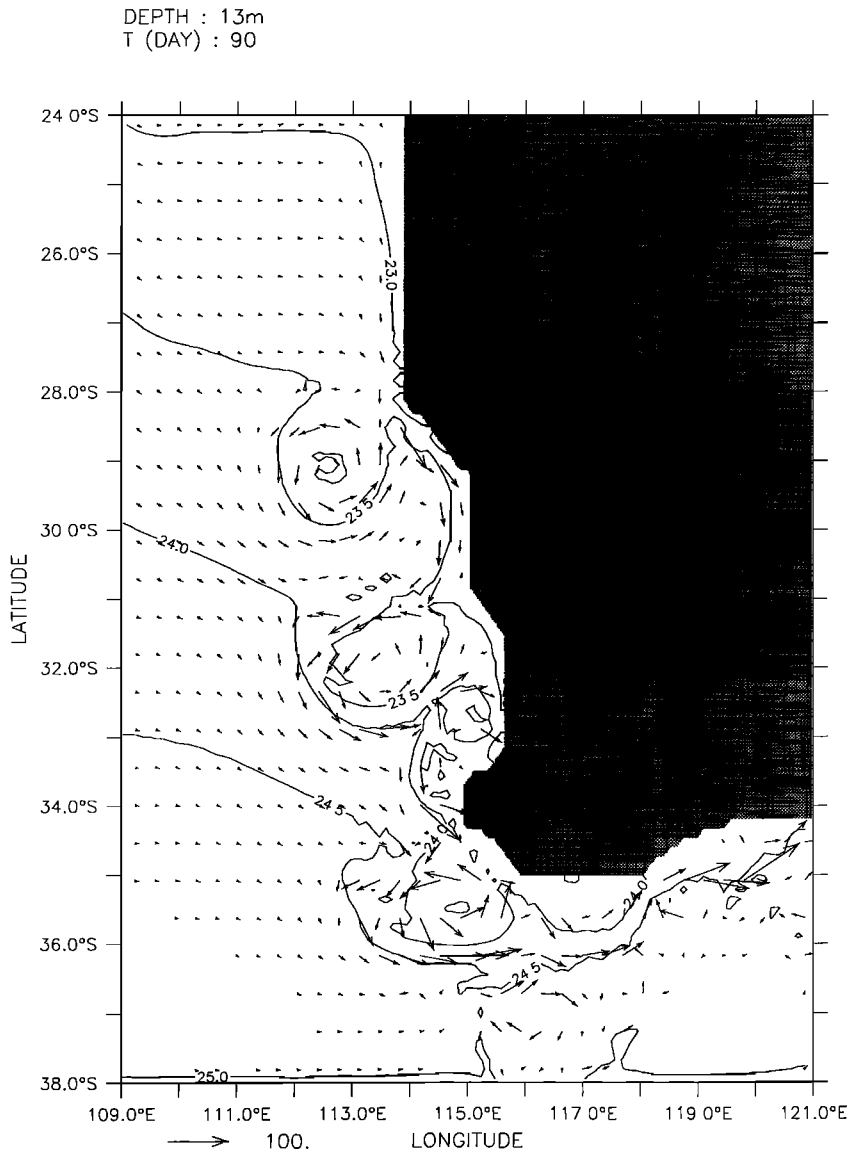

Figure 12. Experiment 1 surface density σ_t field and velocity vectors at day 90. In this and Figure 17, to avoid clutter, velocity vectors are plotted at every fourth grid point in the alongshore and cross-shore directions. The contour interval is 0.5.

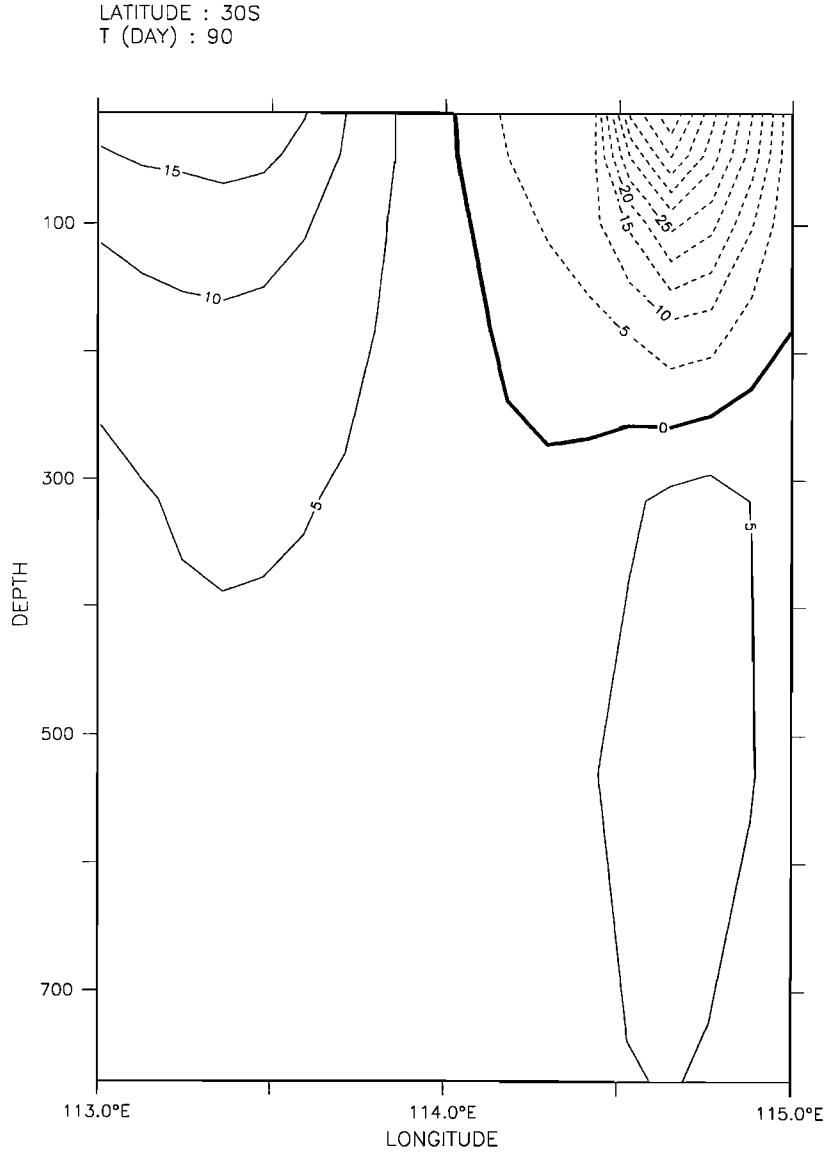

Figure 13. Cross-shore section of velocity field for experiment 1 at day 90. Solid lines indicate equatorward flow, while dashed lines indicate poleward flow. The contour interval is 5 cm s^{-1}.

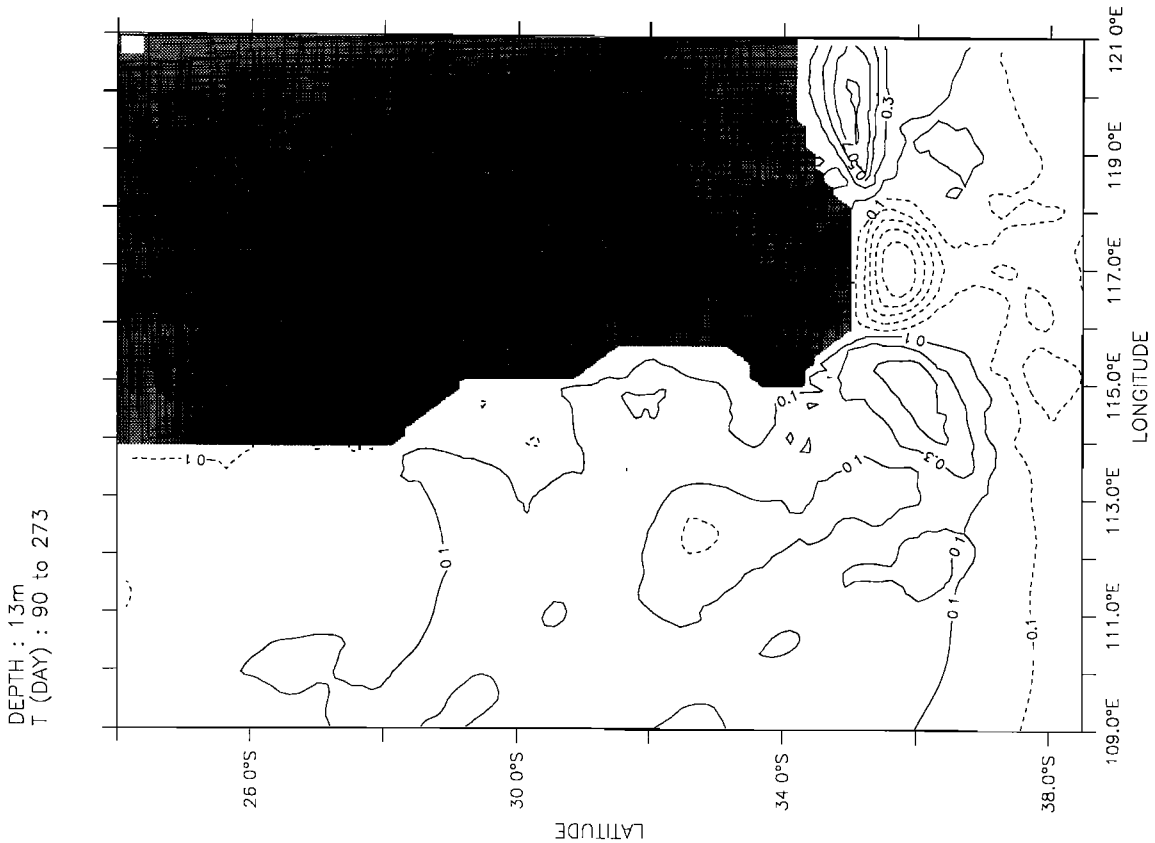

Figure 14b. Same as Figure 14a, but for density $\sigma_{\pm}$, with a contour interval of 0.1.

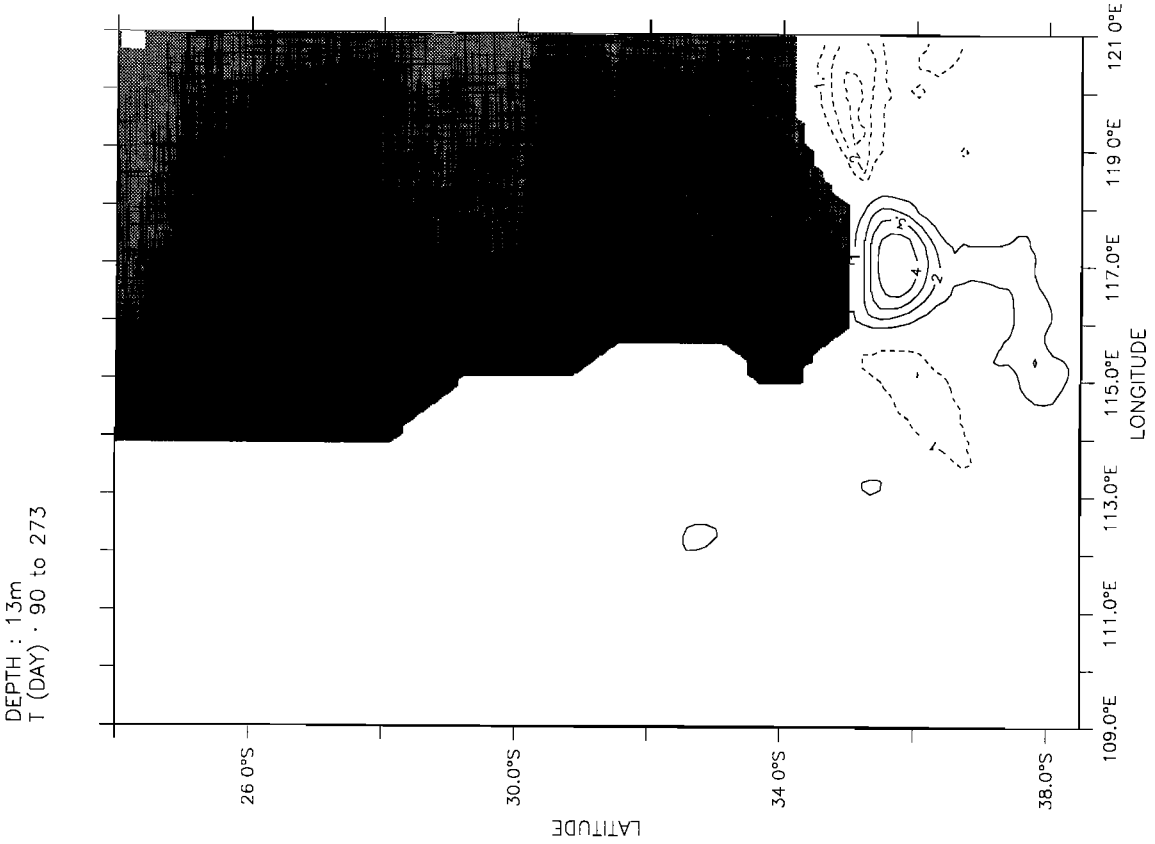

Figure 14a. Difference of time-averaged temperature from April to September (days 90–273) between annual forcing experiments with variable (experiment 1) and uniform (experiment 2) salinity. The contour interval is 1°C.

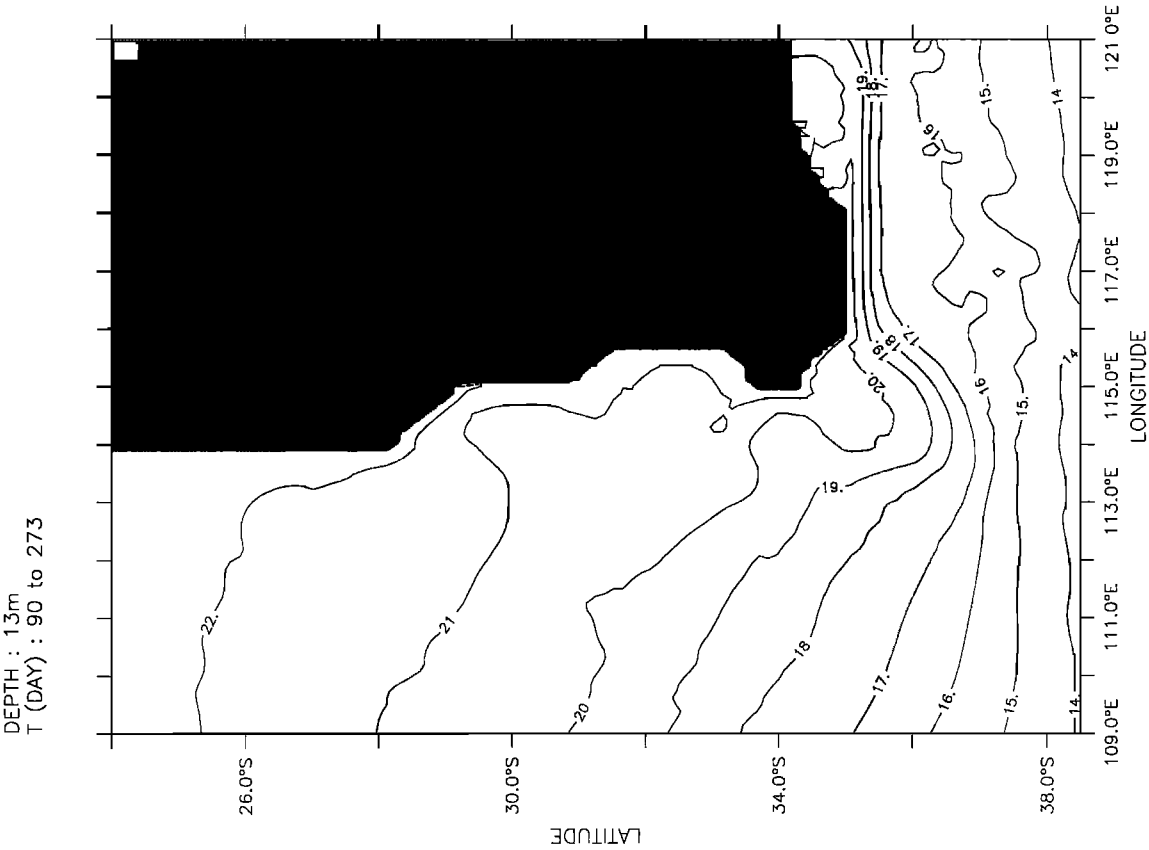

Figure 15b. Same as Figure 15a, but for experiment 2.

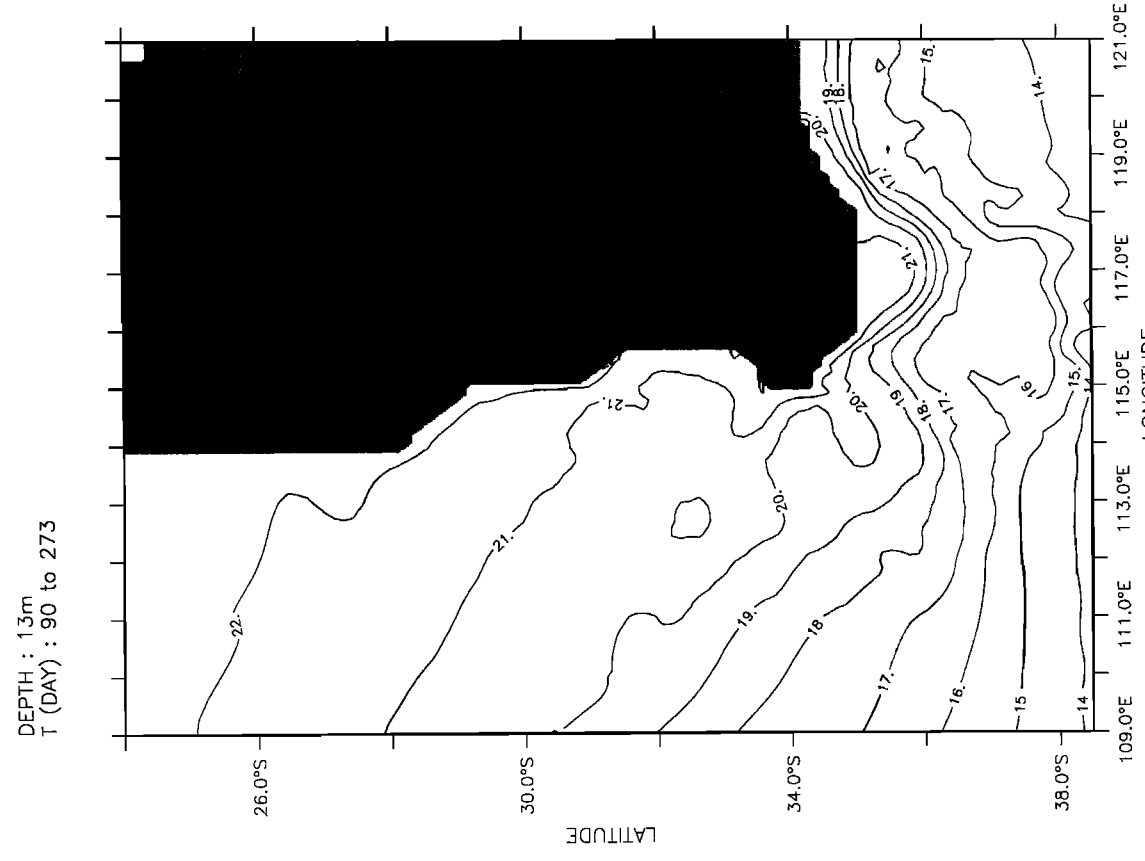

Figure 15a. Time-averaged temperature fields from April to September (days 90–273) for experiment 1. The contour interval is 1°C.

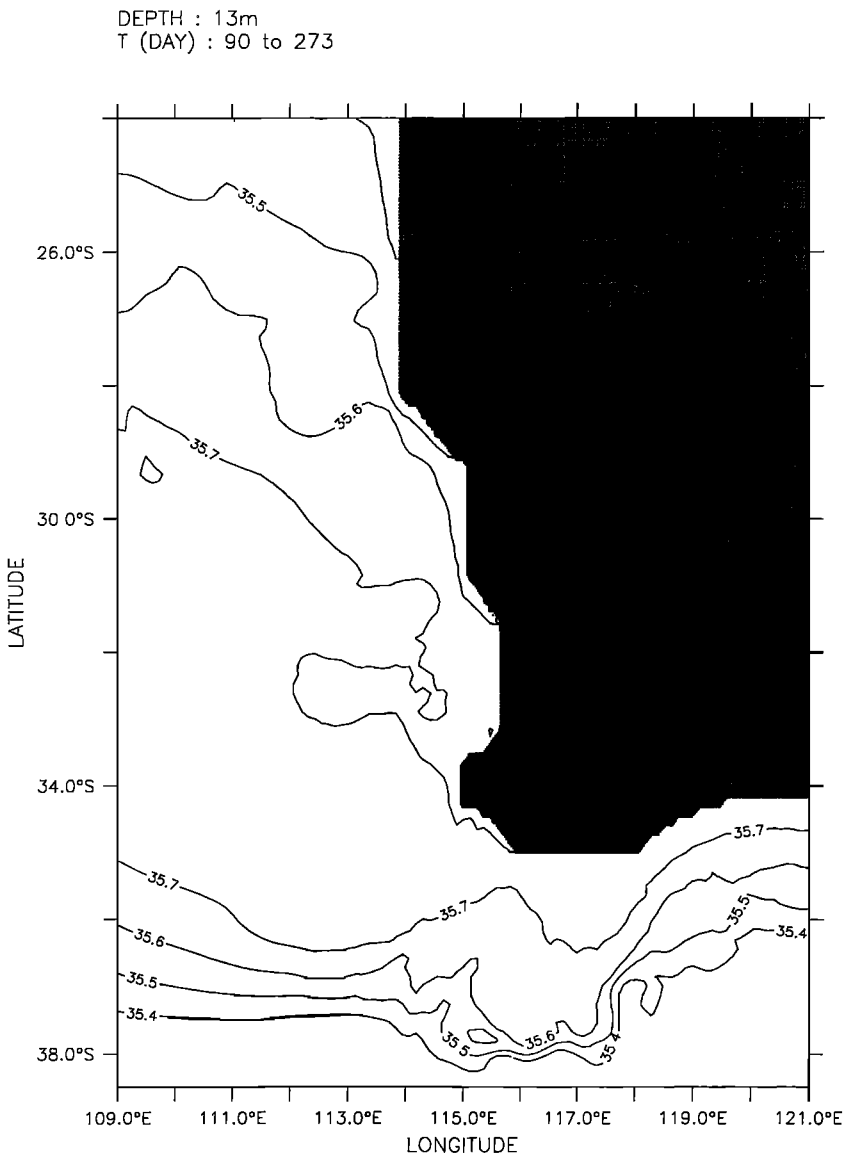

Figure 16. Experiment 1 time-averaged salinity fields from April to September (days 90–273). The contour interval is 0.1 psu.

situation from March on). When the combined effects of thermal and wind forcing on the ocean circulation off Western Australia were investigated, *Batteen et al.* [1992] showed that the effects due to thermal forcing were much greater than those due to wind forcing. In their study, wind forcing effects were only discernible offshore in the equatorward end of the model and did not significantly modify the Leeuwin Current behavior.

In a more recent study by *Batteen and Butler* [1998], climatological temperature fields from *Levitus and Boyer* [1994] were used. In addition, the temperature gradients were continuously applied at the western boundary, and the model domain was expanded to include the southwestern Australian region, an area rich with observations of currents and eddies but lacking in eddy-resolving modeling studies of the region. Model developments included the opening up of the eastern boundary in the vicinity of Esperance in southwestern Australia and the incorporation of an irregular coastline into the model.

In this study, to explore the combined effect of temperature and salinity on the LCS, both annual and seasonal alongshore temperature and salinity fields from *Levitus et al.* [1994] and *Levitus and Boyer* [1994] have been incorporated into the model. In particular, temperature and salinity fields are forced for all 10 levels at the western boundary by annual (experiments 1 and 2) and seasonal (experiments 3 and 4) climatological temperature and salinity data from *Levitus and Boyer* [1994] and *Levitus et al.* [1994]. As in the previous experiments, there is no surface heat flux or mixed layer dynamics, so that changes in the sea surface temperatures are almost entirely due to horizontal advection.

The annual (seasonal) alongshore temperature and salinity fields for the upper five levels (top level), which are assumed to be zonally homogenous, are shown in Figures 10a and 10b (Figures 11a and 11b). For both annual and seasonal forcing conditions, since the lower five levels do not exhibit much horizontal variation, they are assumed to be constant for each

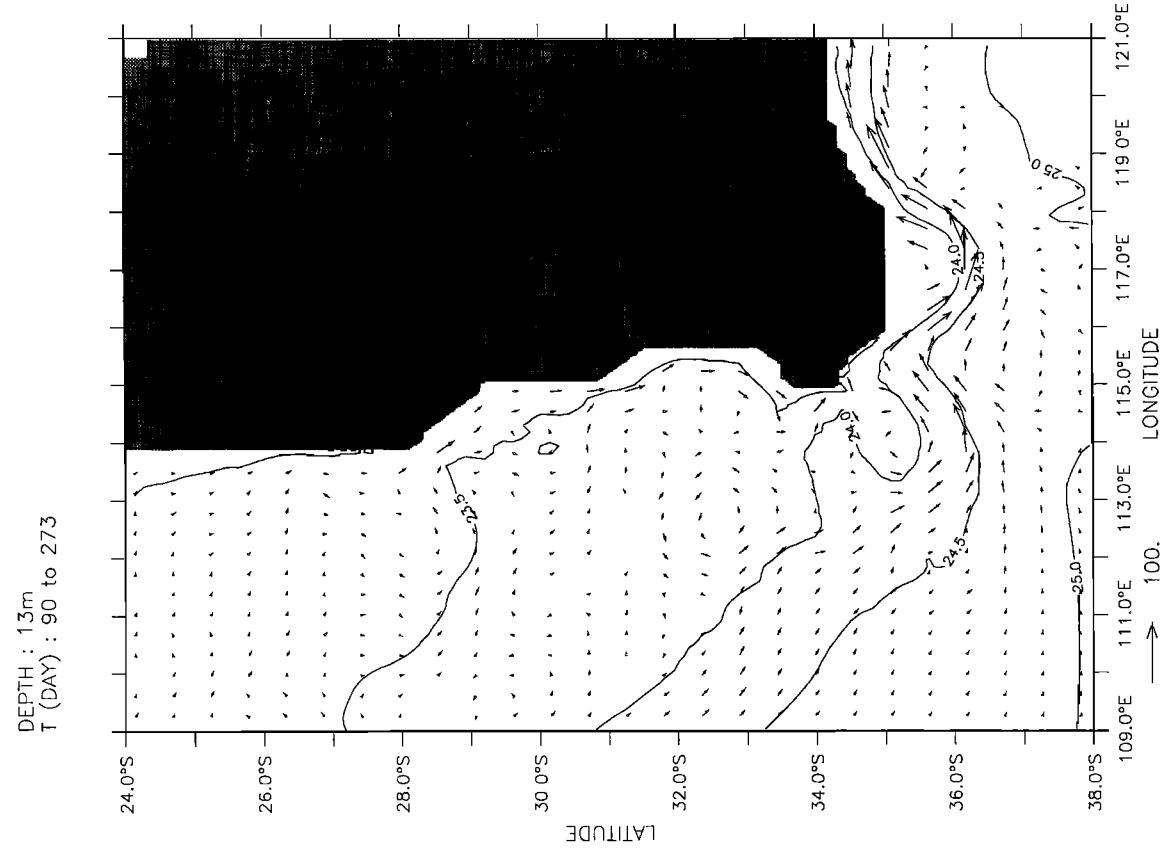

Figure 17a. Time-averaged density σ_t fields and velocity vectors from April to September (days 90–273) for experiment 1. The contour interval is 0.5.

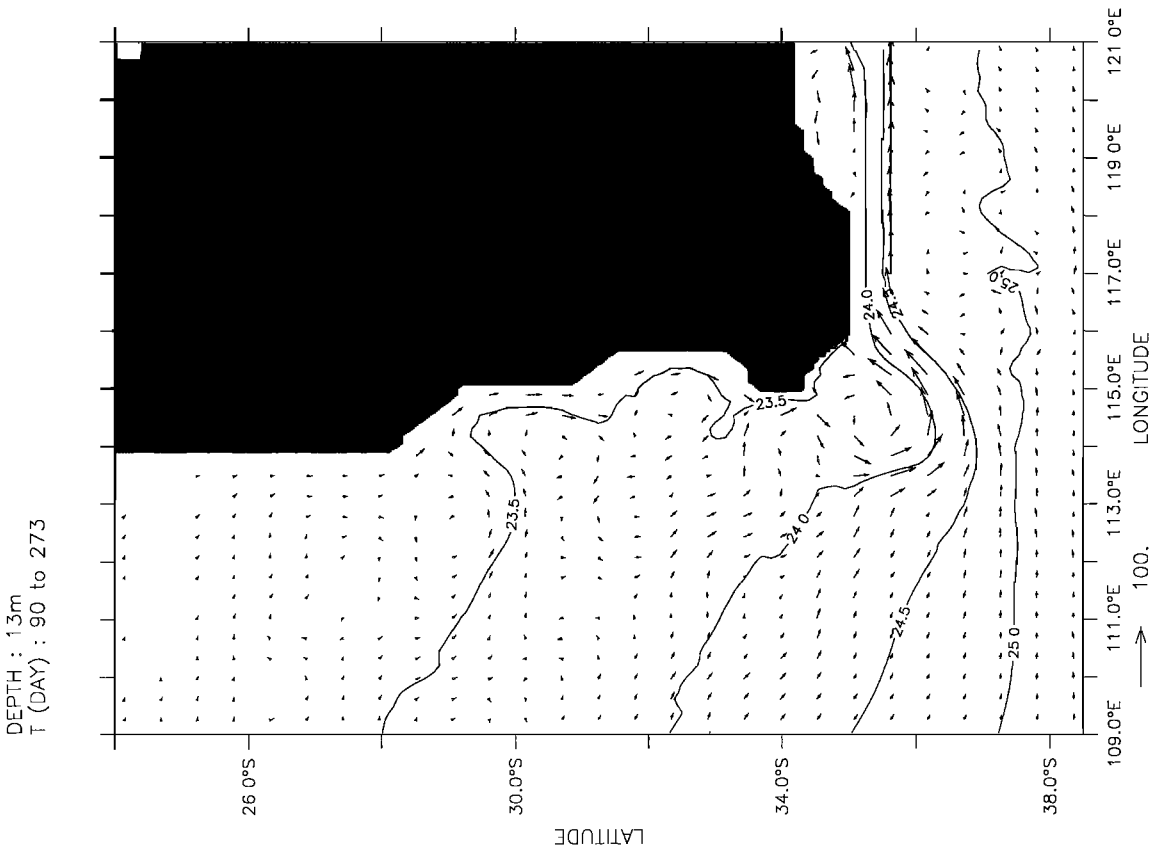

Figure 17b. Same as Figure 17a, but for experiment 2.

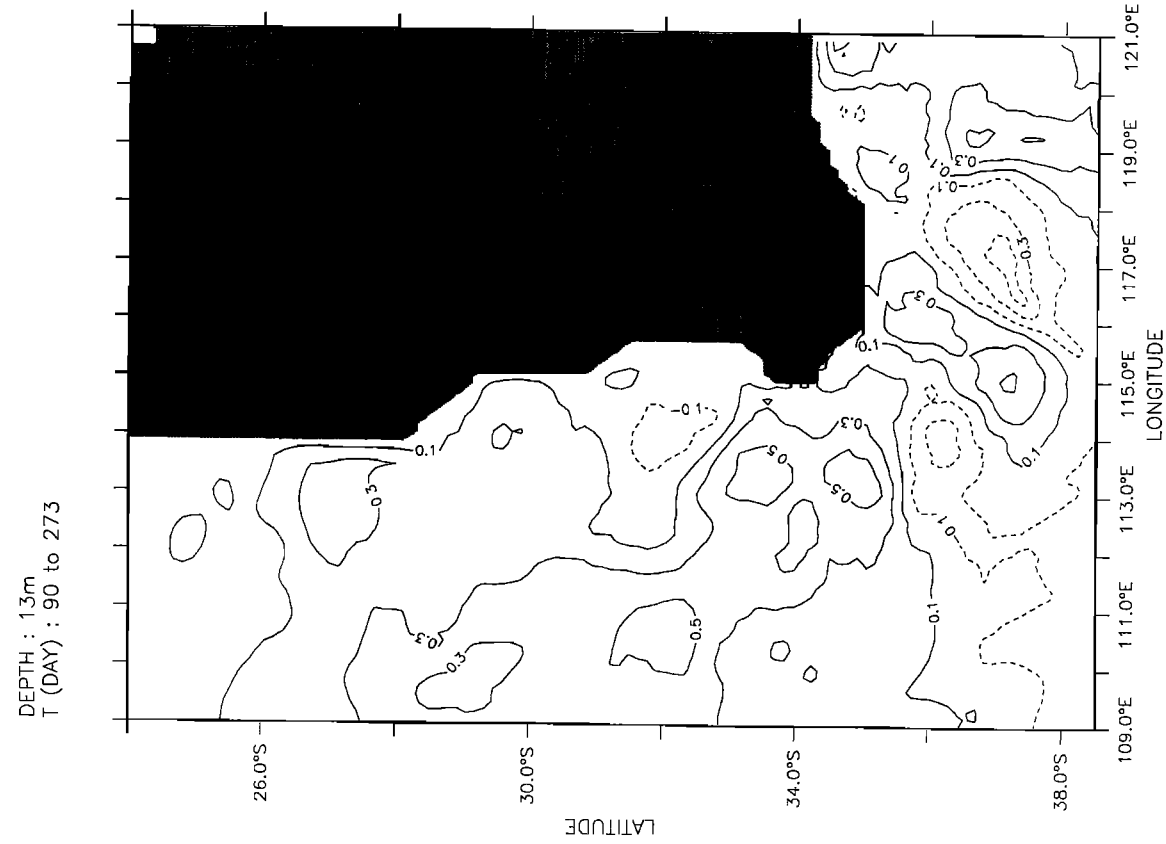

Figure 18b. Same as Figure 18a, but for density σ_t, with a contour interval of 0.1.

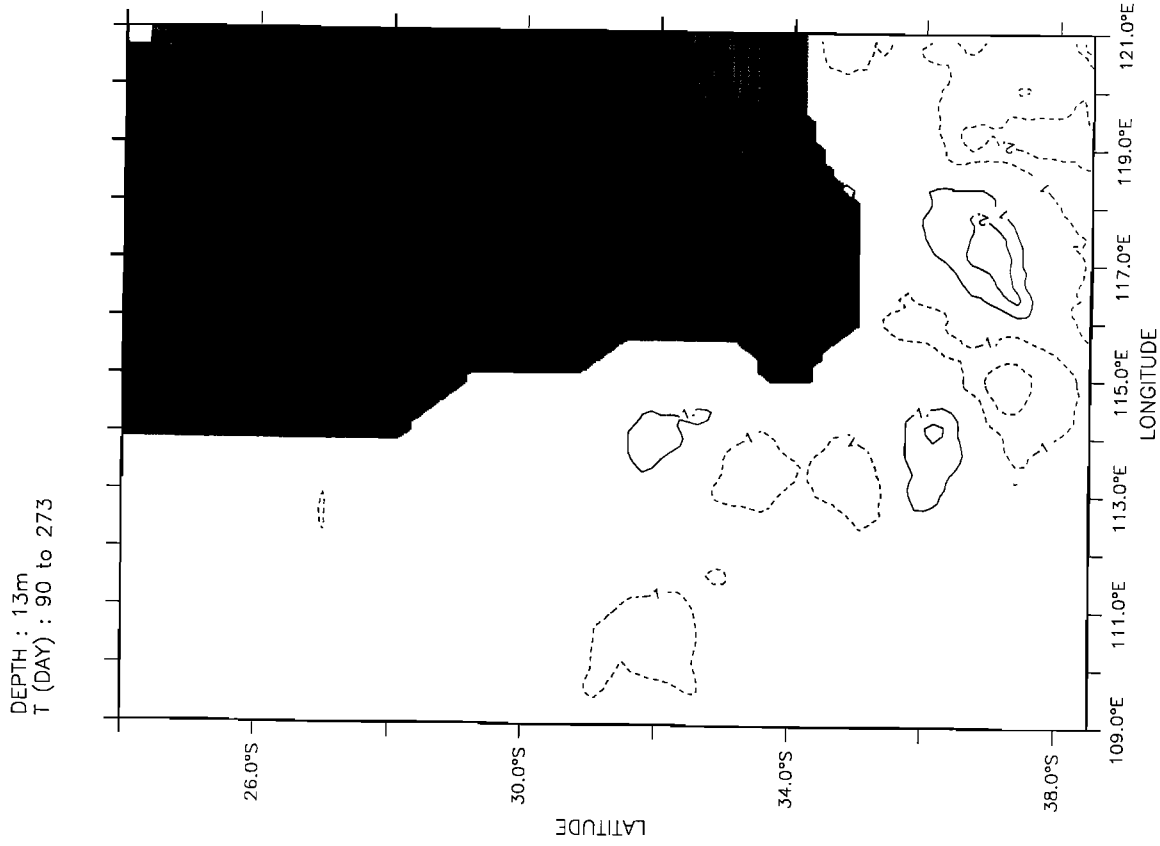

Figure 18a. Difference of time-averaged temperature fields from April to September (days 90–273) between seasonal forcing experiments with variable (experiment 3) and uniform (experiment 4) salinity. The contour interval is 1°C.

level. The temperature values used for levels 6 to 10 are 9.53°C, 6.03°C, 3.24°C, 2.19°C, and 1.27°C. The salinity constant used for the lower five levels is 34.7.

The solid, dashed, and dotted lines plotted in Figures 11a and 11b correspond to latitudinal regions where the three water masses discussed earlier are found. Regardless of the region, the temperature conditions (Figure 11a) indicate that there is, as expected, a temperature maximum in March (austral summer) and a temperature minimum in September (austral winter) throughout the whole region. The salinity conditions (Figure 11b) show relatively strong aperiodic (nonseasonal) variations throughout the year for all of the regions presented.

The design of the model experiments (see Table 1) is as follows. Experiments 1 and 2 study the model response to mean forcing. Experiment 1 uses the variable alongshore temperature and salinity gradient conditions shown in Figures 10a and 10b. Experiment 2 uses the same variable temperature forcing conditions shown in Figure 11a but has salinity set to a constant such that S is replaced by S_0 in (5). Experiments 3 and 4 study the model response to seasonal forcing. Experiment 3 uses the variable temperature and salinity forcing fields shown in Figures 11a and 11b. Experiment 4 uses the same variable temperature forcing conditions shown in Figure 11a, but it has salinity set to a constant such that S is replaced by S_0 in (5).

3.2. Results From Model Simulations

In each of the experiments the model integrations start from a state of rest. Once a day, the model is updated at the western boundary with mean or seasonal temperature and/or salinity fields. Since we are concentrating on the generation of currents and eddies in the LCS due to alongshore temperature and/or salinity gradients, we use results obtained during the first model year over the time period when the Leeuwin Current is strongest (approximately April to September). The results do not change much if the model is run for 2 or 3 years. There is just more westward eddy propagation, which is not an issue here.

Although we are interested in the difference between model runs with variable salinity and with uniform salinity, we first show that the model produces reasonable results. The main phenomena in the LCS are the Leeuwin Current, which flows poleward off Western Australia and eastward off southwestern Australia; an equatorward undercurrent found below the Leeuwin Current off Western Australia; and eddies.

The generation of these features can be explained as follows: owing to the initial alongshore density field, the resulting pressure gradient establishes an onshore geostrophic inflow from the interior of the ocean. As the flow approaches the eastern boundary, it turns and forms a narrow poleward current, the Leeuwin Current, which subsequently enters the Great Australian Bight (Figure 12). Owing to the strong flow of the Leeuwin Current, alongshore temperature gradients are generated at deeper levels, with warm water at the south end of Western Australia and cooler water to the north. These gradients are sufficient to establish an equatorward undercurrent along Western Australia (not shown).

A cross section of meridional velocity (Figure 13) shows the typical structure of the poleward Leeuwin Current and the equatorial undercurrent off Western Australia. The Leeuwin Current jet axis is within ~50 km of the coast and extends from ~200–300 m depth near the coast. Core velocities range from ~30 to 100 cm s^{-1}. A weaker undercurrent with a core velocity of ~5 cm s^{-1} is also seen. The offshore extent of the undercurrent is confined to ~50 km of the coast, while the average core depth is found at ~500 m depth.

Analysis of Figure 13 shows that there is considerable horizontal and vertical shear in the upper layer currents off Western Australia. Barotropic instability can result from horizontal shear in the currents, while baroclinic instability can result from vertical shear in the currents. As a result, both types of instability (mixed) can be present simultaneously. Following the analysis techniques of *Batteen et al.* [1992], energy transfer calculations, which consist of barotropic (mean kinetic energy to eddy kinetic energy) and baroclinic (mean potential energy to eddy potential energy to eddy kinetic energy) components, were performed for the time periods (~days 40–60) when the meanders and eddies developed. Results for the instability analysis (not shown) show that both barotropic and baroclinic (i.e., mixed) instability mechanisms are responsible for the generation of the anticyclonic eddies shown in Figure 12, with the barotropic instability mechanism dominating over the baroclinic instability mechanism.

Figures 12 and 13 show that the Leeuwin Current with velocities of ~30–100 cm s^3, an equatorward undercurrent with core velocities of ~5–15 cm s^{-1}, and anticyclonic eddies (one just south of Shark Bay, one between Dongara and Fremantle, and one in the vicinity of Cape Leeuwin) are reproduced in the model. These results from model runs are qualitatively similar and compare well with available observations of the LCS [e.g., *Boland et al.*, 1988; *Cresswell and Golding*, 1980].

3.2.1. Experiments 1 and 2: Annual alongshore temperature and salinity gradient experiments. The annual forcing model integration with variable salinity (experiment 1) and that with uniform salinity (experiment 2) begin with identical temperature distributions. When the two integrations are compared with each other, significant differences are found, as is illustrated here for the time period that the Leeuwin Current is strongest (approximately April to September, corresponding to model days 90 to 273). Differences of up to 4°C are noted during this time period (Figure 14a; see corresponding density data in Figure 14b) owing to the advection of warmer (21°C or greater) water in experiment 1 by the Leeuwin Current between Cliffy Head and Albany (compare Figure 15a with 15b). Farther east, between Albany and Esperance, the temperature difference of ~3°C in experiment 1 is due to the trapping of warmer water nearshore by the Leeuwin Current.

The time-averaged salinity field (Figure 16) shows that the three major water masses discussed earlier (see Figure 2) are reproduced well in the LCS model; that is, fresh (<35.5) water is found off the northern part of Western Australia, salty (>35.5) water is found offshore of Western Australia and Cape Leeuwin, and fresh (<35.5) water is found to the south.

The time-averaged density fields (Figures 17a and 17b), along with the density difference between experiments 1 and 2 (Figure 14b) show the following. The density differences north of 34°S are relatively small. The water for experiment 1 off the northern part of Western Australia is less dense than that in experiment 2 owing to the combination of warm and fresh water in the region, while offshore of Western Australia, the water for experiment 1 is more dense owing to the combination of salty and warm water.

The largest density differences (Figure 14b) are found between Cape Leeuwin and Esperance. The water off Cape Leeuwin in experiment 1 is more dense than that in experiment

2 owing to the saltier water. The water between Cliffy Head and Albany is less dense in experiment 1 than in experiment 2 owing to the much warmer (up to 4°C) water in the region. The water east of Albany is more dense in experiment 1 than in experiment 2 owing to the saltier water nearshore that has been advected into the region by the Leeuwin Current.

3.2.2. Experiments 3 and 4: Seasonal alongshore temperature and salinity gradient experiments. Since the LCS has significant temporal variability in salinity (see Figure 11b), experiments 3 and 4 are designed to study the model response to seasonal forcing, both using the same alongshore temperature gradients but with variable salinity gradients (experiment 3) and uniform (experiment 4) salinity. As in the previous experiments, here we focus on the difference between the two model runs to identify the salinity effect on density. During the time period that the Leeuwin Current is strongest, differences of up to 2°C are noted (Figure 18a) owing to the displacement of warm, anticyclonic eddies by the Leeuwin Current in the southwestern Australian region.

North of 34°S, the density differences (Figure 18b) show that the water for experiment 3, compared with experiment 4, is less dense off Western Australia and more dense offshore of Western Australia. The water off Cape Leeuwin in experiment 3 is more dense than that in experiment 4 owing to the combination of salty and warm water in the region. The water between Cliffy Head and Albany is less dense owing to the displacement of warm (up to 2°C), anticyclonic eddies by the Leeuwin Current in the region.

4. Summary

This study used climatological temperature and salinity fields to calculate the salinity contribution to density and dynamic height fields in the Leeuwin Current System (LCS). While the temperature gradient is primarily linear, with warmest water to the north, the salinity field is spatially inhomogeneous with low-salinity (tropical) water to the north and northwest, high-salinity (subtropical) water to the southwest, and low-salinity (sub-Antarctic) water to the south. A comparison of annual density fields, calculated with uniform and variable salinity, showed that, off Western Australia, the density field was primarily determined by temperature. South of 34°S, the effect of salinity on density became significant. In particular, off southwestern Australia, the density was shown to be influenced by both the warm and salty (subtropical) water mass and the fresh and cold (sub-Antarctic) water mass. The seasonal density field patterns were found to be similar to the annual density field patterns.

The annual dynamic height fields, calculated with uniform and variable salinity, showed similar flow patterns off Western Australia but different flow patterns between 34°S and 36°S. Throughout the year the seasonal dynamic height fields calculated with uniform and variable salinity showed similar flow patterns off Western Australia and different flow patterns south of 36°S.

In addition to the analysis of the climatological temperature and salinity fields, a high-resolution, multilevel, primitive equation model was used to investigate the role of salinity in the formation of currents and eddies in the LCS. After incorporating salinity into the model, two identical ocean models, one with a climatological salinity field and the other with no horizontal salinity gradients, were run and compared with each other.

Experiments 1 and 2 used mean alongshore temperature and salinity gradients to initialize and force the model. Despite the model runs being initialized with the same temperature distributions, differences of up to 4°C were noted during the time period that the Leeuwin Current was strongest in the southwestern Australian region owing to the advection of warmer water by the Leeuwin Current between Cliffy Head and Albany. Large density differences were also found between Cape Leeuwin and Esperance, where the salinity effect on density became significant.

Experiments 3 and 4 used seasonal alongshore temperature and salinity gradients to initialize and force the model. During the time period that the Leeuwin Current was strongest, differences of up to 2°C were noted in the southwestern Australian region owing to the displacement of warm, anticyclonic eddies by the Leeuwin Current nearshore. Large density differences were also found between Cape Leeuwin and Albany, where the salinity effect on density became significant.

The results from both the climatological analysis and the model experiments strongly suggest that there are important quantitative differences between uniform and variable salinity calculations, particularly in the Cape Leeuwin and southwestern Australian regions. The low- and high-salinity tags in the LCS are found to be particularly useful for identifying the contributions of the different water masses to the development of the Leeuwin Current and eddies.

Acknowledgments. This work was supported by the National Science Foundation under grant OCE-9203325 and by direct funding at the Naval Postgraduate School, with the office of Naval Research as the sponsor. We wish to thank the reviewers for comments that helped to improve the text. We also wish to thank Mike Cook for his computer assistance with Figure 1 and Phaedra Green for editorial assistance.

References

Andrews, J. C., Eddy structure and the West Australian Current, *Deep Sea Res.*, *24*, 1133–1148, 1977.

Arakawa, A., and V. R. Lamb, Computational design of the basic dynamical processes of the UCLA general circulation model, in *Methods in Computational Physics*, vol. 17, edited by J. Chang, pp. 173–265, Academic, San Diego, Calif., 1977.

Batteen, M. L., Wind-forced modeling studies of currents, meanders, and eddies in the California Current System, *J. Geophys. Res.*, *102*, 985–1010, 1997.

Batteen, M. L., and C. L. Butler, Modeling studies of the Leeuwin Current off Western and Southern Australia, *J. Phys. Oceanogr.*, in press, 1998.

Batteen, M. L., and Y.-J. Han, On the computational noise of finite-difference schemes used in ocean models, *Tellus*, *33*, 387–396, 1981.

Batteen, M. L., and M. J. Rutherford, Modeling studies of eddies in the Leeuwin Current: The role of thermal forcing, *J. Phys. Oceanogr.*, *20*, 1484–1520, 1990.

Batteen, M. L., R. L. Haney, T. A. Tielking, and P. G. Renaud, A numerical study of wind forcing of eddies and jets in the California Current System, *J. Mar. Res.*, *47*, 493–523, 1989.

Batteen, M. L., M. J. Rutherford, and E. J. Bayler, A numerical study of wind- and thermal-forcing effects on the ocean circulation off Western Australia, *J. Phys. Oceanogr.*, *22*, 1406–1433, 1992.

Batteen, M. L., C. A. Collins, C. R. Gunderson, and C. S. Nelson, The effect of salinity on density in the California Current System, *J. Geophys. Res.*, *100*, 8733–8749, 1995.

Boland, F. M., J. A. Church, A. M. G. Forbes, J. S. Godfrey, A. Huyer, R. L. Smith, and N. J. White, Current-meter data from the Leeuwin Current Interdisciplinary Experiment, *Rep. 198*, Aust. Mar. Lab., Commonw. Sci. and Ind. Res. Organ., Hobart, Tasmania, 1988.

Camerlengo, A. L., and J. J. O'Brien, Open boundary conditions in rotating fluids, *J. Comput. Phys.*, *35*, 12–35, 1980.

Cresswell, G. R., and T. J. Golding, Observations of a south-flowing

current in the southeastern Indian Ocean, *Deep Sea Res., Part A, 27A*, 449–466, 1980.

Gentilli, J., Thermal anomalies in the eastern Indian Ocean, *Nature Phys. Sci., 238*, 93–95, 1972.

Godfrey, J. S., and K. R. Ridgway, The large-scale environment of the poleward-flowing Leeuwin Current, Western Australia: Longshore steric height gradients, wind stresses and geostrophic flow, *J. Phys. Oceanogr., 15*, 481–495, 1985.

Haney, R. L., A numerical study of the response of an idealized ocean to large-scale surface heat and momentum flux, *J. Phys. Oceanogr., 4*, 145–167, 1974.

Hirst, A. C., and J. S. Godfrey, The role of Indonesian Throughflow in a global ocean GCM, *J. Phys. Oceanogr., 23*, 1057–1086, 1993.

Holland, W. R., The role of mesoscale eddies in the general circulation of the ocean—Numerical experiments using a wind-driven quasi-geostrophic model, *J. Phys. Oceanogr., 8*, 363–392, 1978.

Holland, W. R., and M. L. Batteen, The parameterization of subgrid scale heat diffusion in eddy-resolved ocean circulation models, *J. Phys. Oceanogr., 16*, 200–206, 1986.

Levitus, S., Climatological atlas of the world ocean, *NOAA Prof. Pap. 13*, 173 pp., U.S. Dep. of Commer., Washington, D.C., 1982.

Levitus, S., and T. P. Boyer, World ocean atlas 1994, vol. 4, Temperature, *NOAA Atlas NESDI 4*, 117 pp., U.S. Dep. of Commer., Washington, D. C., 1994.

Levitus, S., R. Burgett, and T. P. Boyer, World ocean atlas 1994, vol. 3, Salinity, *NOAA Atlas NESDI 3*, 99 pp., U.S. Dep. of Commer., Washington, D. C., 1994.

McCreary, J. P., Jr., S. R. Shetye, and P. K. Kundu, Thermohaline forcing of eastern boundary currents: With application to the circulation off the west coast of Australia, *J. Mar. Res., 44*, 71–92, 1986.

Pearce, A. F., and G. R. Cresswell, Ocean circulation off Western Australia and the Leeuwin Current, *Inf. Serv. Sheet 16-3*, 4 pp., Div. of Oceanogr., Commonw. Sci. and Indus. Res. Organ., North Beach, Western Australia, July 1985.

Pickard, G. L., and W. J. Emery, *Descriptive Physical Oceanography*, 5th ed., 320 pp., Pergamon, Tarrytown, N. Y., 1990.

Rochford, D. J., Seasonal variations in the Indian Ocean along 110 degrees E, I, Hydrological structure of the upper 500 m, *Aust. J. Mar. Freshwater Res., 20*, 1–50, 1969.

Rochford, D. J., Seasonal changes in the distribution of Leeuwin Current waters off Southern Australia. *Aust. J. Mar. Freshwater Res., 37*, 1–10, 1986.

Smith, R. L., A. Huyer, J. S. Godfrey, and J. A. Church, The Leeuwin Current off Western Australia, 1986–1987, *J. Phys. Oceanogr., 21*, 323–345, 1991.

Thompson, R. O. R. Y., Observations of the Leeuwin Current off Western Australia, *J. Phys. Oceanogr., 14*, 623–628, 1984.

Thompson, R. O. R. Y., Continental-shelf-scale model of the Leeuwin Current, *J. Mar. Res., 45*, 813–827, 1987.

Weatherly, G. L., A study of the bottom boundary layer of the Florida Current, *J. Phys. Oceanogr., 2*, 54–72, 1972.

Weaver, A. J., and J. H. Middleton, On the dynamics of the Leeuwin Current, *J. Phys. Oceanogr., 19*, 626–648, 1989.

M. L. Batteen and M.-J. Huang, Department of Oceanography, Naval Postgraduate School, Code OC/BV, Monterey, CA 93943. (e-mail: batteen@oc.nps.navy.mil)

(Received December 31, 1996; revised December 15, 1997; accepted March 5, 1998.)